SUPPLEMENTAL FIGURES

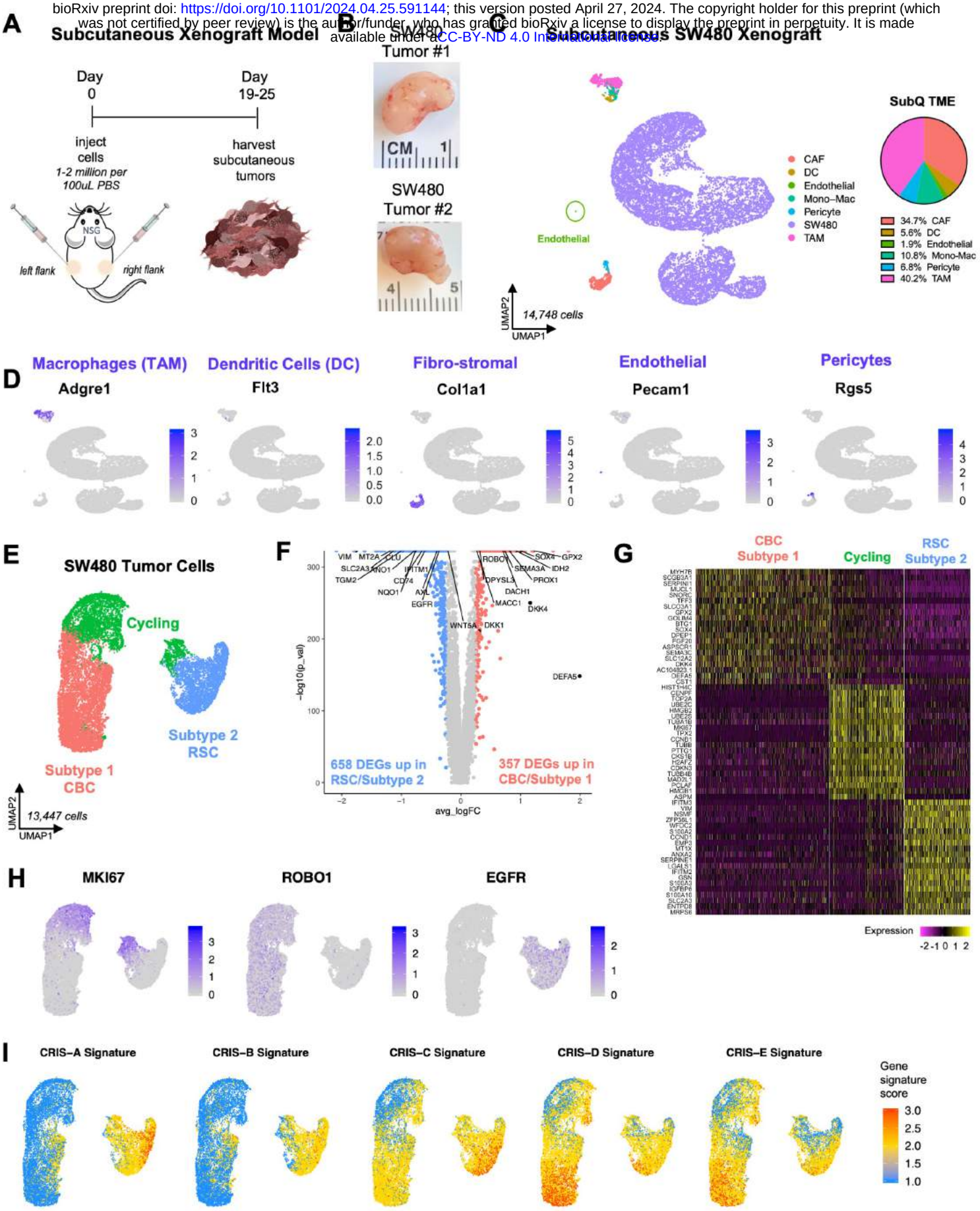

Figure S1, related to Figure 1: The human tumor compartment of SW480 subcutaneous xenografts is comprised of two subtypes.

Figure S1, related to Figure 1: The human tumor compartment of SW480 subcutaneous xenografts is comprised of two subtypes.

A: Schematic diagram of the subcutaneous xenograft model and tumor development. B: Images of the two SW480 subcutaneous tumors before tissue dissociation and scRNA-seq. C: UMAP clustering of all mouse and human cells captured in SW480 subcutaneous (SubQ) xenografts with pie chart showing the average proportion of cell types in the SubQ TME. D: Gene expression plots of cell type biomarkers in the SubQ TME. E: UMAP clustering of human tumor cells reveals two distinct populations, Subtype 1 (CBC) and Subtype 2 (RSC). F: Volcano Plot highlights significant differentially expressed genes in CBC/Subtypes 1 and RSC/Subtype 2. G: Heatmap of marker genes distinguishing tumor subtype clusters. H: Gene expression plots of subtype-specific biomarkers (*ROBO1* marks the CBC phenotype, *EGFR* marks the RSC subtype, MKI67 marks the cycling cells in both subtypes). I: Gene signature plots of CRC patient-derived CRIS molecular subtype signatures.

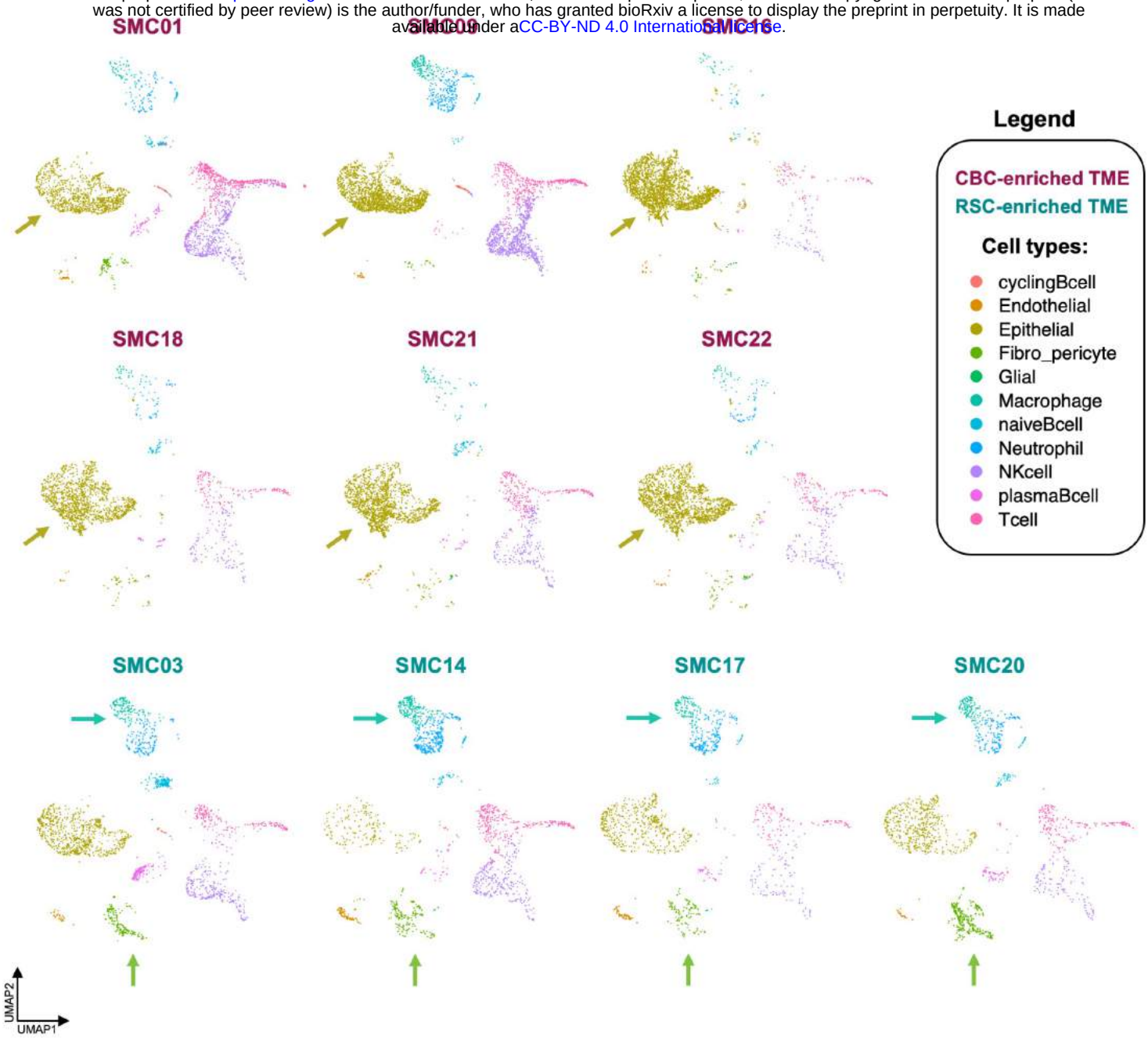

Figure S2 related to Figure 2: CRC patients exhibit different TME compositions associated with CBC and RSC phenotypes.

UMAP clustering of scRNA-seq data from Korean (SMC) patient tumor biopsies. Patients in maroon have tumors with strong CBC signatures and contain a larger proportion of epithelial cells (gold arrow). Patients in teal have strong RSC signatures and contain a larger proportion of stromal fibroblast-pericytes (green arrow) and myeloid immune cell types (macrophages and neutrophils, blue arrow).

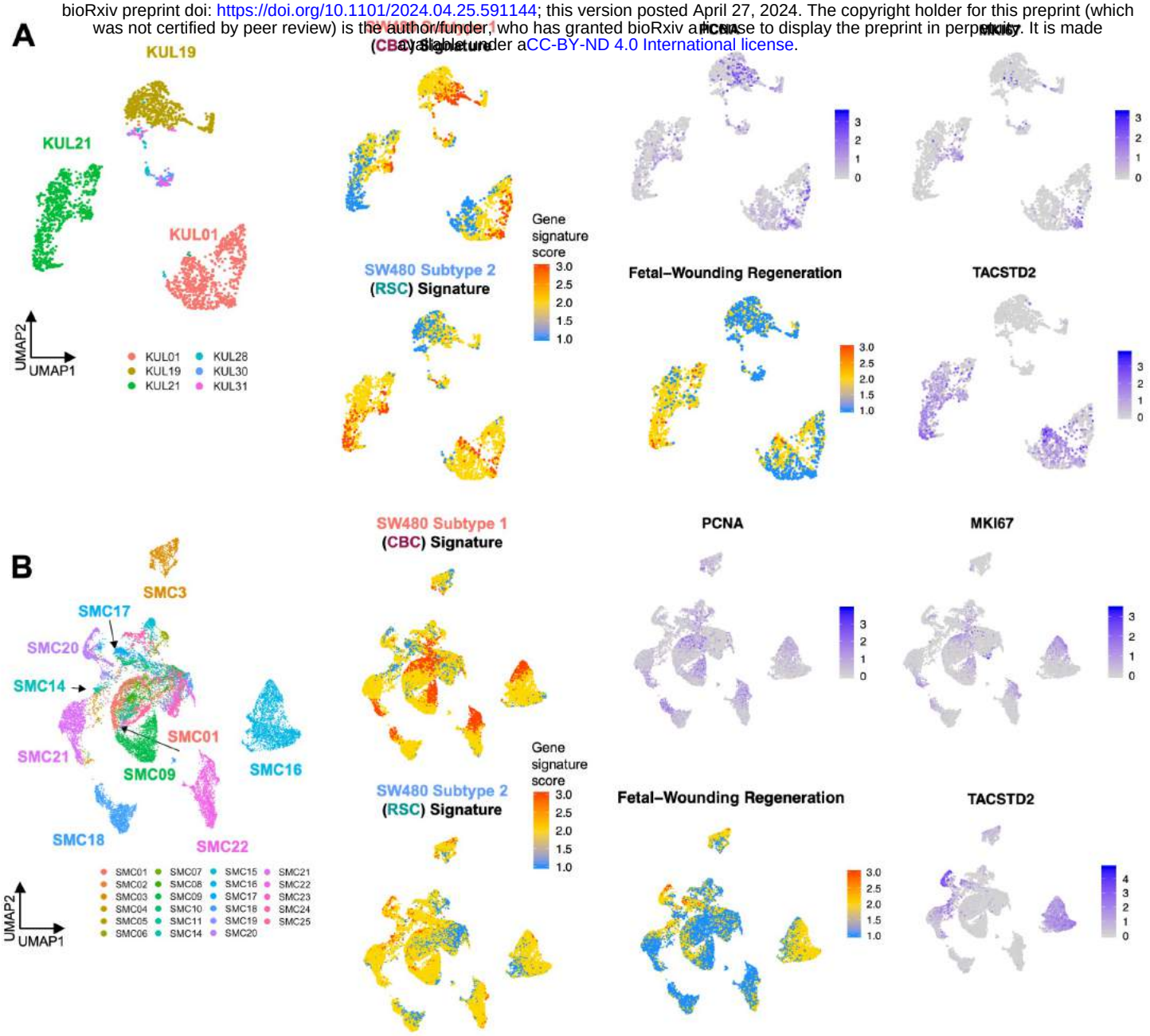

Figure S3, related to Figure 2: CRC stem cell subtype signatures co-exist in most patients in varying proportions. UMAPs of Belgian/KUL (A) and Korean/SMC (B) patients published in Lee et al., 2020, with gene expression and signature plots distinguishing stem cell subtypes.

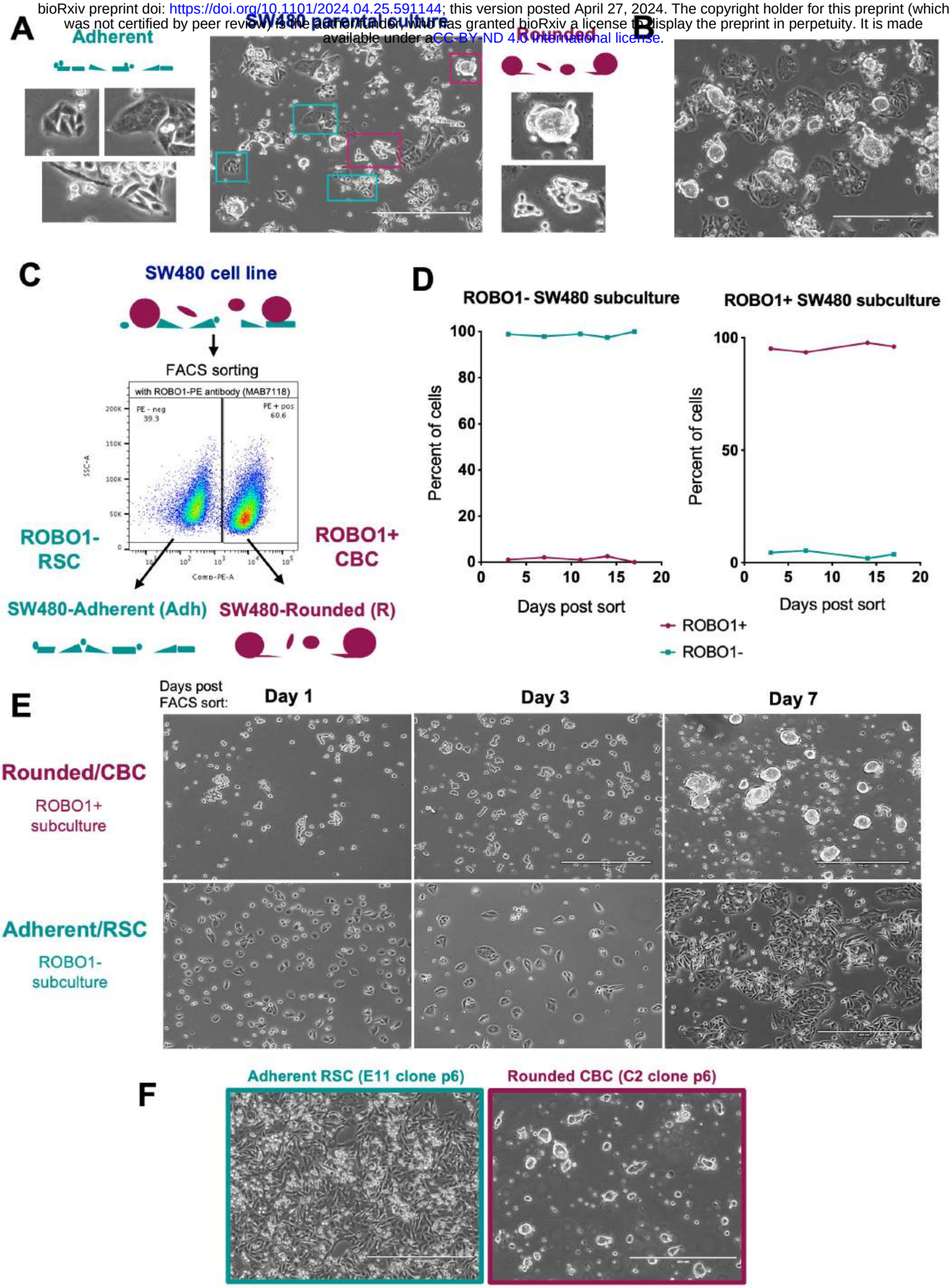

Figure S4, related to Figure 3: Use of ROBO1 expression as a novel sorting strategy to isolate SW480 stem cell subtypes.

Figure S4, related to Figure 3: Use of ROBO1 expression as a novel sorting strategy to isolate SW480 stem cell subtypes.

A-B: Phase contrast images of the SW480 culture with magnified insets showing a mixture of cellular morphologies, scale = 400µm. C: Fluorescence Activated Cell Sorting (FACS) using ROBO1-PE antibodies separates two populations of morphologies (Adherent versus Rounded). D: Flow Cytometry Analysis of subcultured ROBO1+ and ROBO1- sorted cells retain positive and negative cell surface expression of ROBO1, respectively. E: Phase contrast images of ROBO1+ Rounded/CBC and ROBO1- Adherent/RSC subcultures days after FACS sorting from the parental SW480 culture, scale = 400µm. F: Phase contrast images of single cell clonal derivations of Adherent/RSC (E11 clone) and Rounded/CBC (C2) cultures; scale = 400µm.

A

Reference STRs

Sample Name	D5S818	D13S317	D7S820	D16S539	VWA	TH01	AMEL	TPOX	CSF1PO	Multiple Profiles Seen	Match Comments
R+-positive SW480-CBC	13 13	12 12	8 8	13 13	16 16	8 8	X X	11 11	13 14	No	Sample matches SW 480 above the 80% match threshold. This is considered a match to SW 480 (GNE).
R--negative SW480-RSC	13 13	12 12	8 8	13 13	16 16	8 8	X X	11 11	13 14	No	Sample matches SW 480 above the 80% match threshold. This is considered a match to SW 480 (GNE).

Additional STRs

Sample Name	D3S1358	D21S11	D18S51	Penta_E	Penta_D	D8S1179	FGA
R+-positive	15 15	30 30.2	13 13.0	10 10.0	9 15	13 13	24 24
R--negative	15 15	30 30.2	no amp	no amp	9 9	13 13	24 24

B

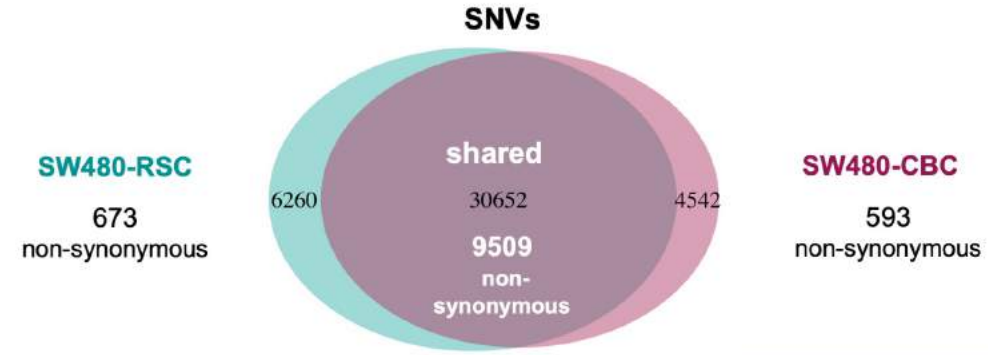

C

known mutation reported by ATCC

Chromosome	Region	Type	Reference	Allele	Genotype	Homo sapiens (hg19)_Gene	Amino acid change	Non-synonymous
17	7576921	SNV	G	A	A	TP53	ENSP00000391127:p.Pro309Ser; ENSP00000269305:p.Pro309Ser; ENSP00000398846:p.Pro309Ser; ENSP00000352610:p.Pro309Ser; ENSP00000425104:p.Pro177Ser; ENSP00000391478:p.Pro309Ser	Yes
17	7577120	SNV	C	T	T	TP53	ENSP00000269305:p.Arg273His; ENSP00000391127:p.Arg273His; ENSP00000391478:p.Arg273His; ENSP00000352610:p.Arg273His; ENSP00000398846:p.Arg273His; ENSP00000425104:p.Arg141His	Yes
17	7579472	SNV	G	C	C	TP53	ENSP00000391478:p.Pro72Arg; ENSP00000269305:p.Pro72Arg; ENSP00000426252:p.Pro72Arg; ENSP00000473895:p.Pro72Arg; ENSP00000398846:p.Pro72Arg; ENSP00000352610:p.Pro72Arg; ENSP00000424104:p.Pro72Arg; ENSP00000410739:p.Pro72Arg; ENSP00000391127:p.Pro72Arg	Yes
5	112175303	SNV	C	T	T	APC, CTC-554D6.1	ENSP00000257430:p.Gln1338*; ENSP00000427089:p.Gln1338*; ENSP00000413133:p.Gln1338*	Yes
5	112176756	SNV	T	A	A	APC, CTC-554D6.1	ENSP00000413133:p.Val1822Asp; ENSP00000427089:p.Val1822Asp; ENSP00000257430:p.Val1822Asp	Yes
12	25398284	SNV	C	A	A	KRAS	ENSP00000452512:p.Gly12Val; ENSP00000256078:p.Gly12Val; ENSP00000451856:p.Gly12Val; ENSP00000308495:p.Gly12Val	Yes
2	85360829.. 85360831	Deletion	GGC	-	-	TCF7L1	ENSP00000282111:p.Gly14del	Yes
5	38527308	SNV	G	A	A	LIFR	ENSP00000263409:p.His116Tyr; ENSP00000398368:p.His116Tyr; ENSP00000426685:p.His116Tyr	Yes

Figure S5, related to Figure S4: STR profiling and exomic sequencing confirm a common SW480 origin with identical cancer driver mutations in CBC and RSC subtypes.

A: Cell line authentication report of short tandem repeat (STR) profiling in ROBO1+ sorted (R+-positive) SW480-CBC and ROBO1- sorted (R—negative) SW480-RSC cells. B: Venn diagram summary of the total number of single nucleotide variations (SNV) and of those that encode non-synonymous protein mutations, generated from exomic sequencing of SW480-RSC and SW480-CBC subtypes. C: Table of shared SNV mutations in both SW480 subtypes, both RSC and CBC cells contain the same cancer driver mutations in *TP53, APC,* and *KRAS* gene loci.

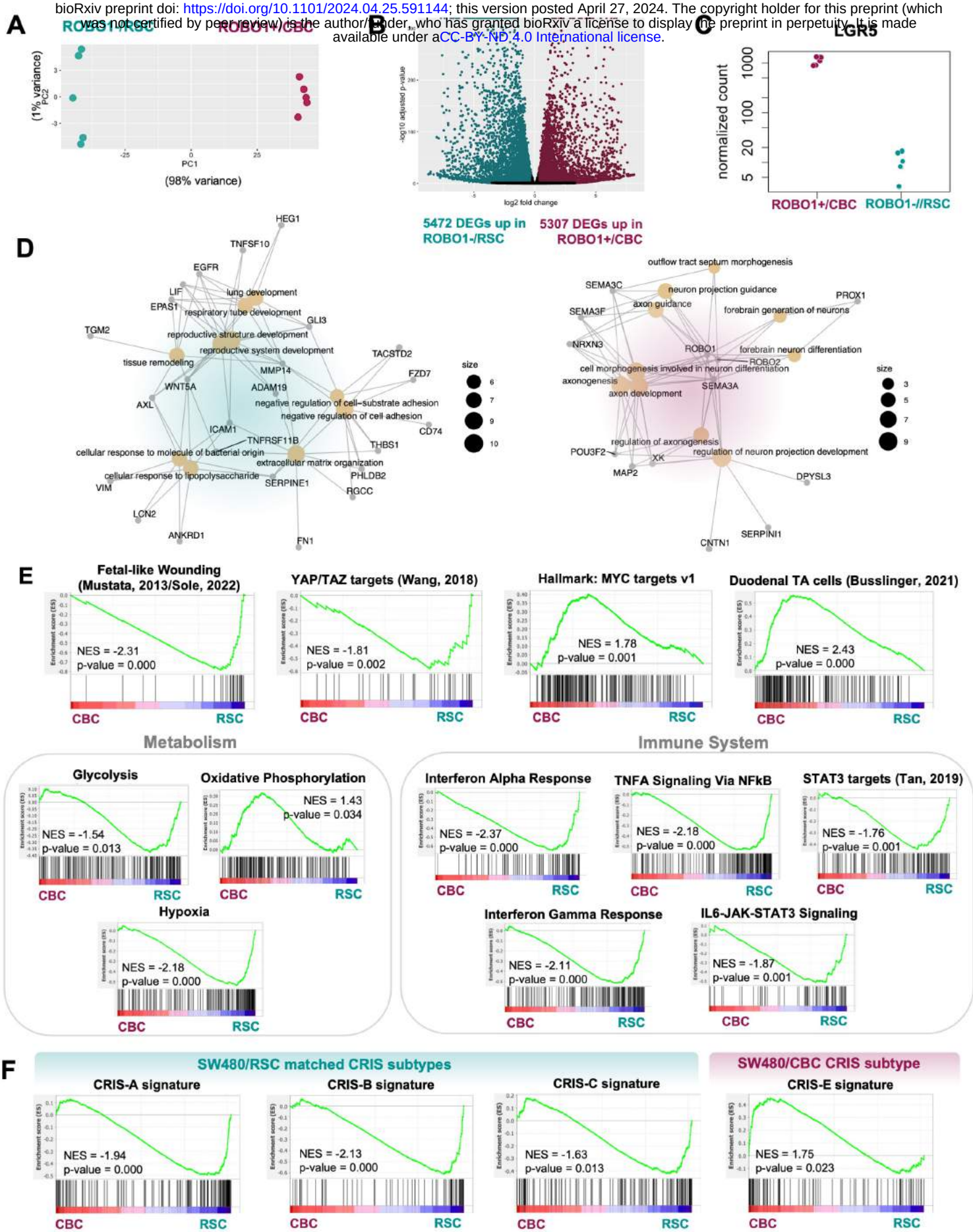

Figure S6, related to Figure 3/Figure S4: SW480 subtypes have different transcriptional profiles that align with distinct binary classifications and human colorectal cancer CRIS subtypes.

Figure S6, related to Figure 3/Figure S4: SW480 subtypes have different transcriptional profiles that align with distinct binary classifications and human colorectal cancer CRIS subtypes.

A: Principal component analysis plot comparing transcriptomes of ROBO1+/CBC and ROBO1-/RSC sorted cells by bulk RNA sequencing, n = 5. B: Volcano Plot highlights thousands of significant DEGs in RSC/ROBO1- sorted cells and CBC/ROBO1+ sorted cells. C: LGR5 mRNA expression in each sorted replicate, n=5. D: Top marker genes (logFC>3) expressed in RSC/ROBO1- cells (left) and CBC/ROBO1+ cells (right) are linked to different GO biological processes; top DEGs in RSC cells were linked to biological processes such as extracellular matrix production, cell adhesion and cytoskeleton regulation while CBC DEGs align with neuronal processes such as axon guidance and neuronal differentiation. E: Gene Set Enrichment Analysis (GSEA) using MSigDB hallmarks, GO biological processes, and published gene signatures distinguish CBC from RSC cells. F: Gene Set Enrichment Analysis (GSEA) of the CRC patient-derived gene signatures show subtype-specific alignment to distinct CRIS molecular subtypes (see Supplemental Data 3 for gene lists).

A

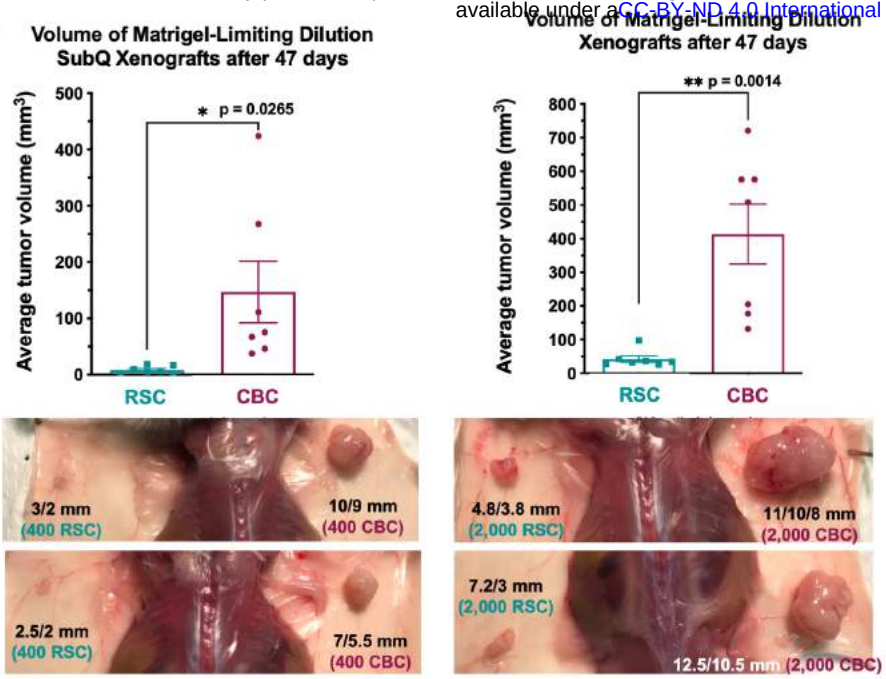

B

Number of cells injected	RSC	CBC
250,000 (PBS)	n = 3/3	n = 3/3
50,000 (PBS)	n = 3/3	n = 3/3
10,000 (PBS)	n = 1/4	n = 2/4
2,000 (PBS)	n = 0/4	n = 0/4
10,000 (Matrigel/PBS)	n = 4/4	n = 4/4
2,000 (Matrigel/PBS)	n = 7/7	n = 7/7
400 (Matrigel/PBS)	n = 5/7	n = 7/7

Figure S7, related to Figure 3: SW480 subtypes have similar tumor initiating potential but CBC cells form larger tumors.

A: Representative images and weights of limiting dilution subcutaneous (SubQ) xenograft experiments injecting 400 cells (A) or 2,000 cells (B) per inoculant. B: Summary of limiting dilution experiments injecting smaller numbers of cells down to a minimum number in PBS or Matrigel/PBS.

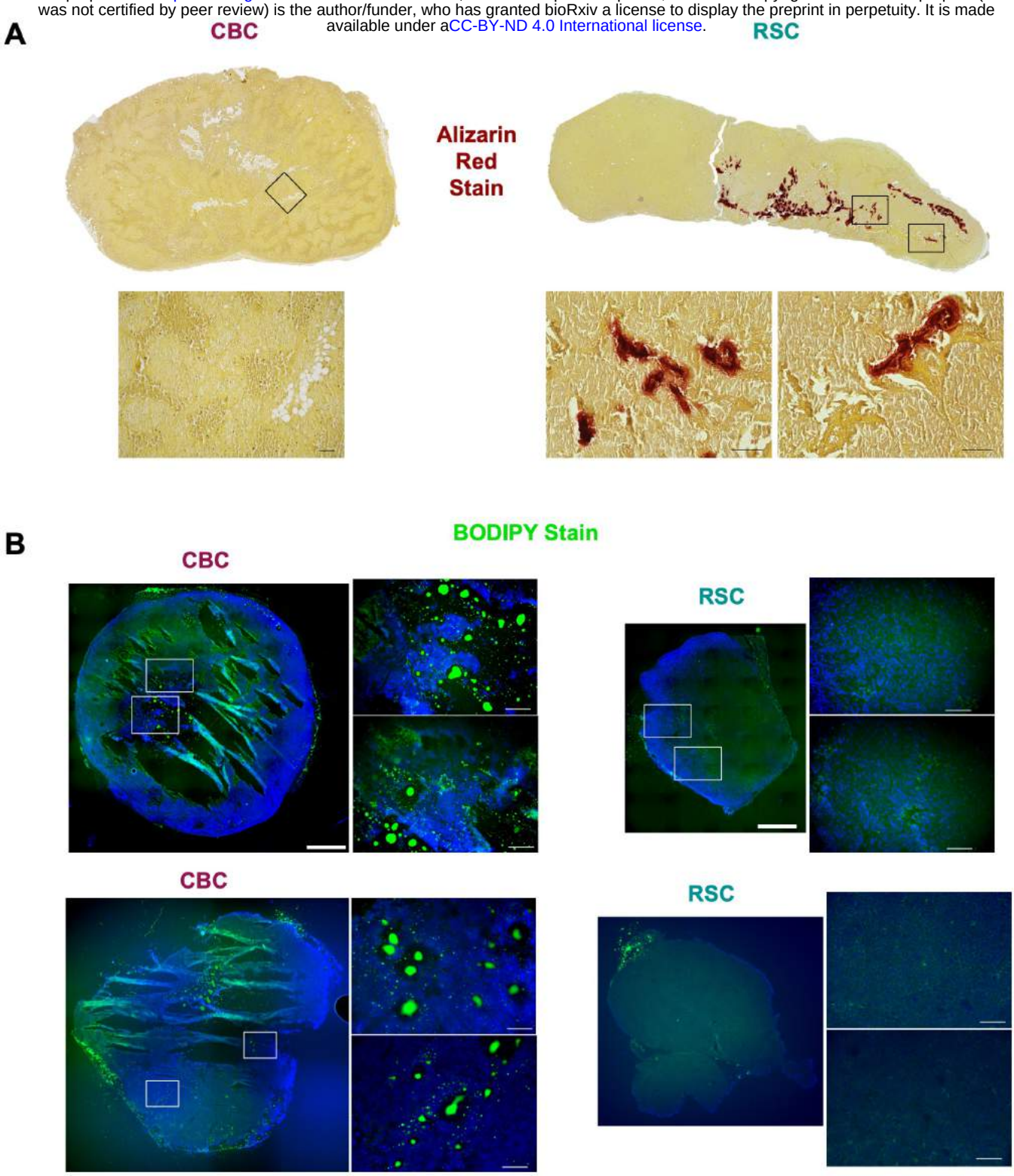

Figure S8, related to Figure 3: Diverse stromal features of osteogenesis in RSC tumors and adipogenesis in CBC tumors.

A: Alizarin Red staining marks areas of calcium-deposited tissue (a surrogate for bone-associated extracellular matrix) found only in SW480-RSC tumors, with magnified images of tumor core below (CBC inset = 10X and RSC insets = 20X), scale = 100μm. B: BODIPY staining illuminates lipid droplets (a biomarker of adipocytes) inside the tumor core of CBC tumors, with 20X magnified images on right, scale = 1mm and 100μm (20X).

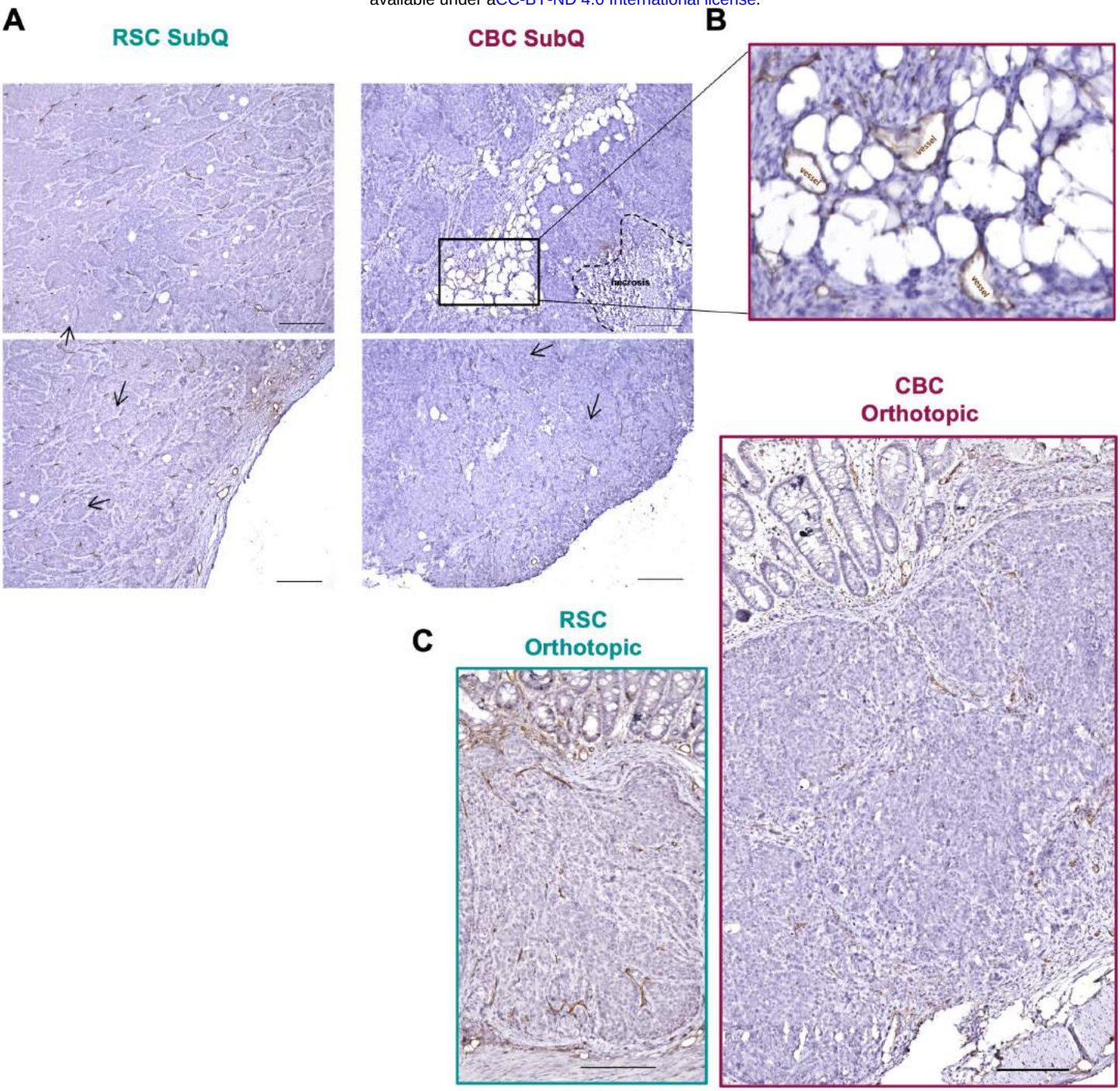

Figure S9, related to Figures 3 and 4: RSC tumors demonstrate increased vascularization in both xenograft models.

A: Immunohistochemistry staining for Cd31+ vasculature in subcutaneous (SubQ) tumors, arrows point to examples of vessels, scale = 200μm. B: Magnified image of the CBC tumor core identifies few Cd31 vessels within an adipogenic core. C: Immunohistochemistry staining for Cd31+ vasculature in orthotopic tumors marks thicker vessels infiltrating RSC tumors, scale = 200μm.

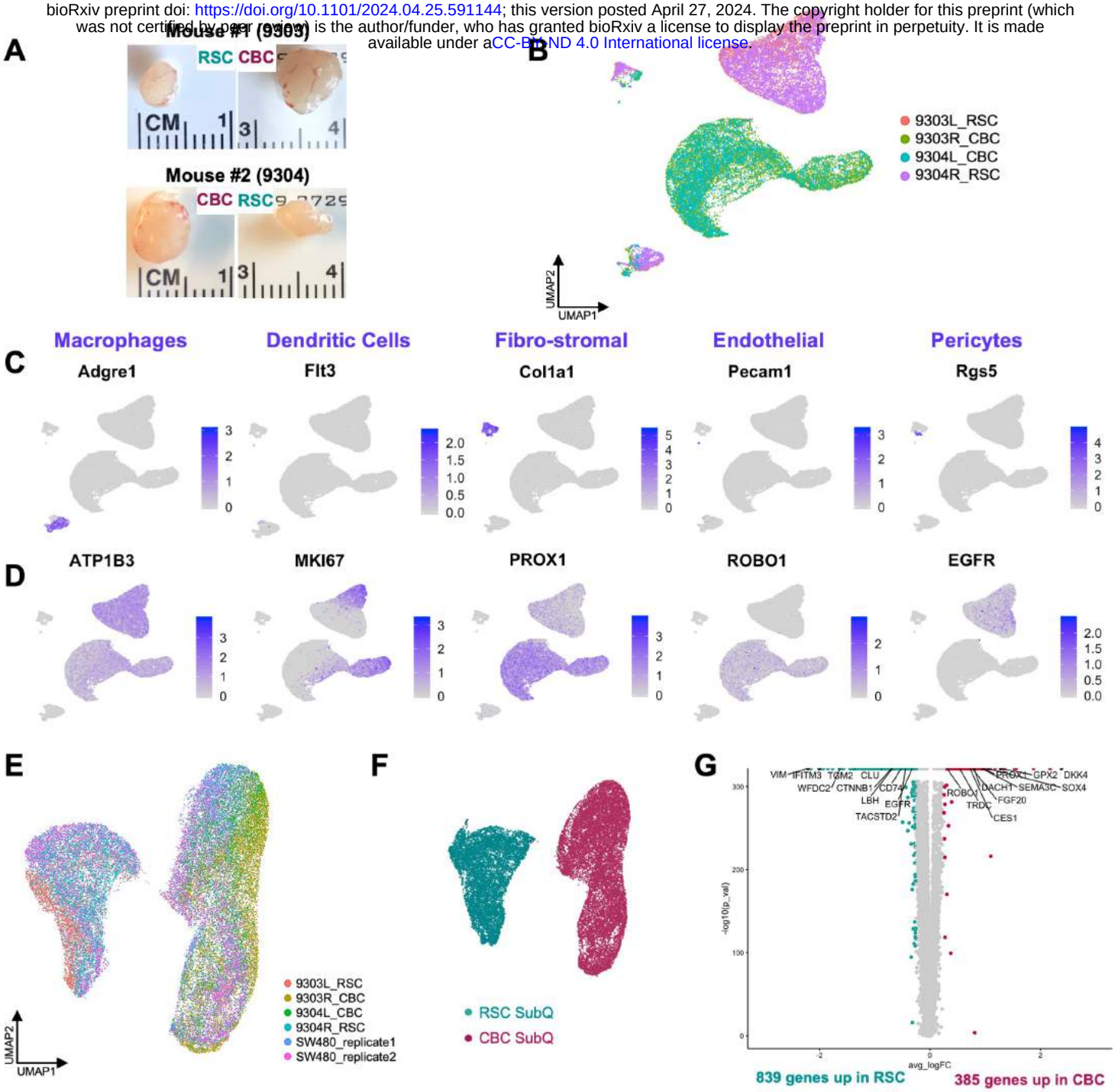

Figure S10, related to Figure 3: Stromal, immune and human tumor populations are transcriptionally distinct in RSC and and CBC subcutaneous tumors.

A: Images of subcutaneous (SubQ) xenograft tumors prior to tissue dissociation for scRNA-seq. B: UMAP clustering of all mouse and human cells from CBC and RSC SubQ tumors, n = 2 each subtype. C: Gene expression plots of marker genes for various cell types found in the SubQ TME. D: Gene expression plots of human biomarkers (human specific antigen CD298 (*ATP1B3*), cell cycle marker (*MKI67*+) and subtype-specific biomarkers (*PROX1, ROBO1, EGFR*)). E: UMAP clustering of human tumor cells from SW480 subtype-specific and mixed xenografts (from Figure S1), colored by tumor ID. The clustering of CBC and RSC cells in SubQ tumors propagated as separate xenografts (i.e. as right/left flank tumors in the same mouse, e.g. mice 9303 and 9304) were nearly identical to their transcriptomic signatures when mixtures of both cell subtypes were propagated in a single xenograft (e.g. SW480_replicates), suggesting tumor signatures are strongly intrinsic. F: UMAP of human tumor cells, colored by subtype-specific xenograft. G: Volcano Plot highlights significant differentially expressed genes (DEGs) in RSC versus CBC cells in SubQ xenografts (positive logFC values represent genes upregulated in CBC cells, negative logFC values represent genes upregulated in RSC cells; for top 100 DEG lists for each subtype see Supplemental Data 3).

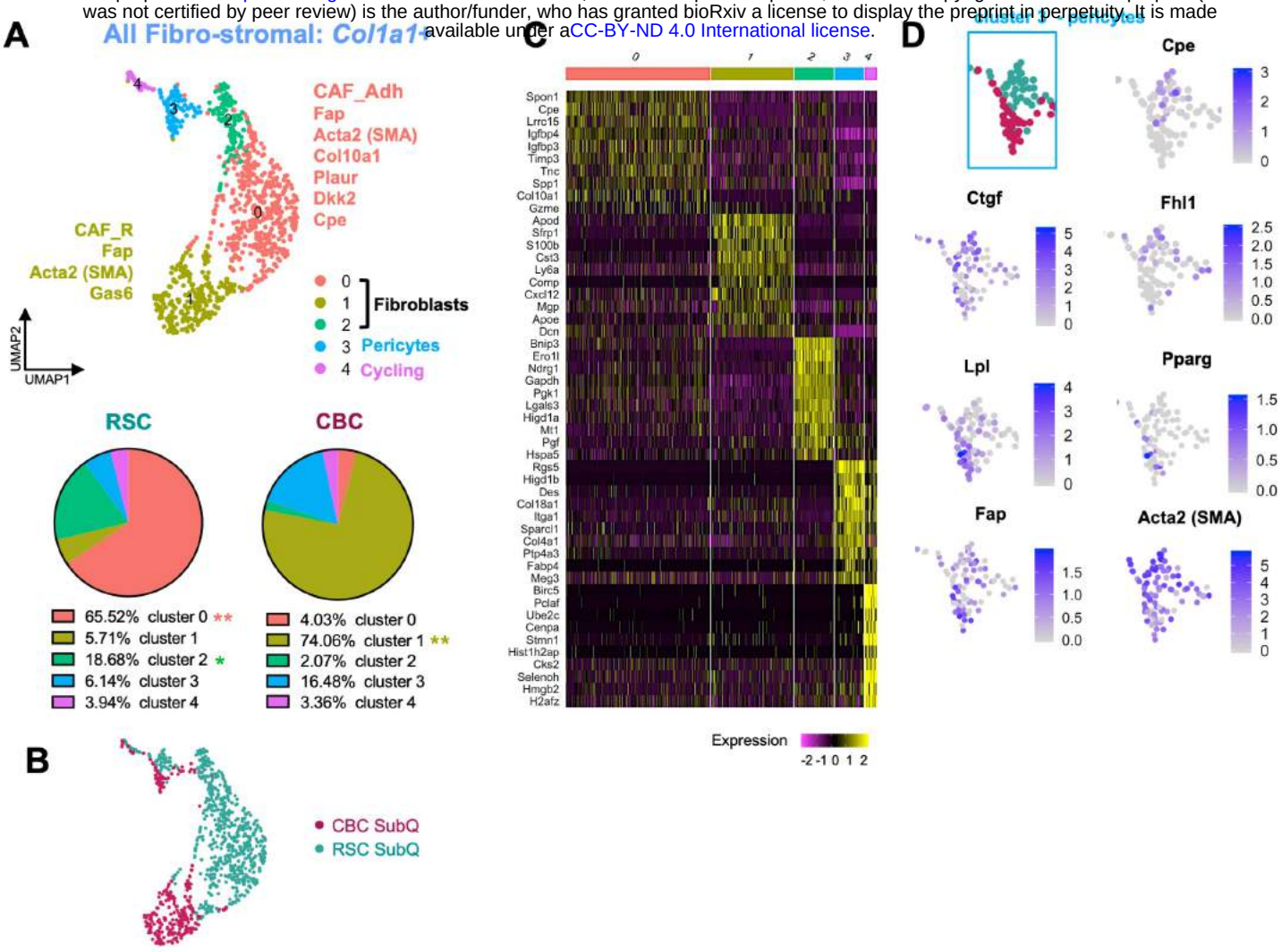

Figure S11, related to Figure 3: Fibroblasts and pericytes have distinct transcriptional profiles in CBC and RSC subcutaneous tumors.

A: UMAP clustering of *Col1a1+* expressing stromal cells in subcutaneous (SubQ) tumors, with pie charts showing significant differences in proportional composition between tumor subtypes. B: UMAP of fibro-stromal cells colored by subtype-specific xenograft. C: Heatmap of marker genes expressed in the different fibro-stromal clusters. D: UMAP crop of the pericyte cluster colored by tumor subtype xenograft and with corresponding gene expression plots of fibroblast (*Fap, Acta2*), adipocyte (*Lpl, Pparg*), and osteoblast (*Ctgf, Cpe, Fhl1*) related marker genes. P values = * < 0.05, ** < 0.01 (Student's t test).

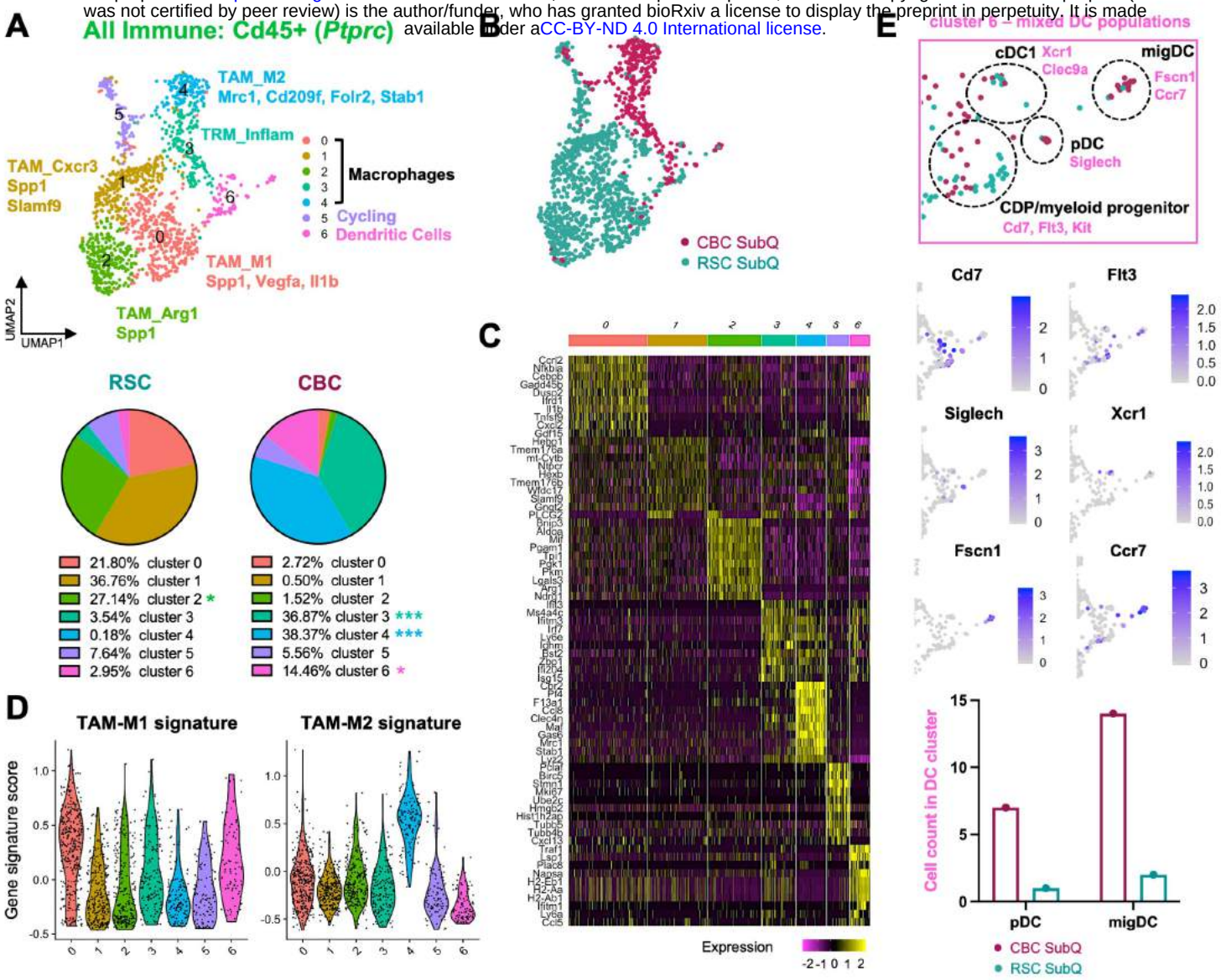

Figure S12, related to Figure 3: Tumor associated macrophages and dendritic cell populations have distinct profiles in CBC and RSC subcutaneous tumors.

A: UMAP clustering of *Cd45+* immune cells in subcutaneous (SubQ) tumors, with pie charts showing significant proportional differences in clusters between tumor subtypes; Tumor associated macrophage (TAM) states are distinct clusters from Tissue-resident macrophages (TRM). B: UMAP of immune cells colored by subtype-specific xenograft. C: Heatmap of marker genes for immune clusters. D: Violin plot of gene signature scoring for M1 and M2 associated TAM marker genes amongst immune clusters. E: UMAP crop of the dendritic cell (DC) cluster, colored by subtype-specific xenograft, with gene expression plots of biomarkers of DC sub-populations: common DC progenitor (CDP), plasmacytoid DC (pDC), conventional DC 1 (cDC1), and migratory DCs (migDC). Bar plot highlights enriched populations of pDCs and migDCs in CBC xenografts. P values = * < 0.05, *** < 0.001 (Student's t test).

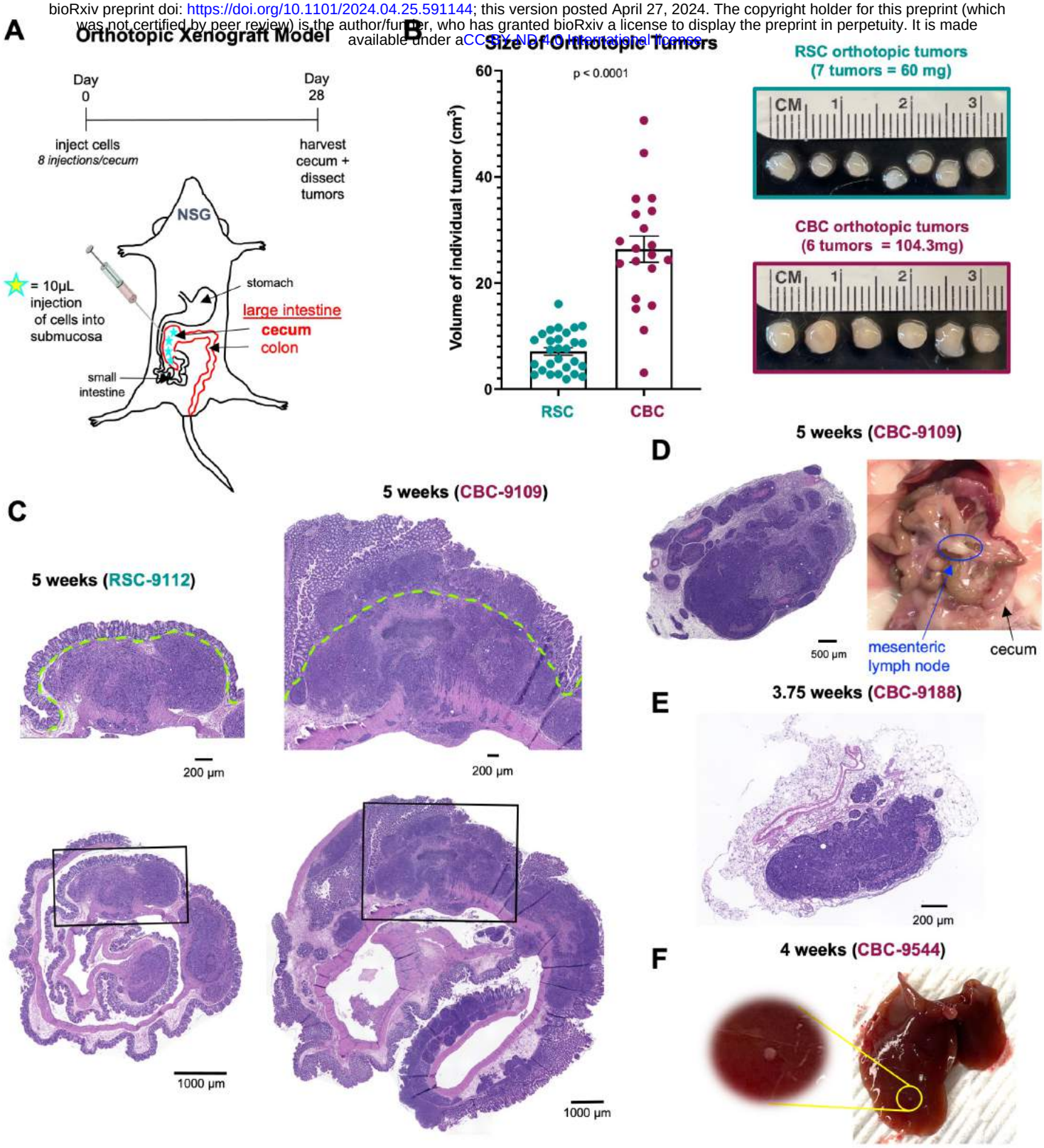

Figure S13, related to Figure 4: The CBC subtype displays a more invasive phenotype in orthotopic xenografts. A: Schematic of the orthotopic tumor model diagramming multi-injections into the cecum of NSG mice and duration of experiment. B: Average size of individual orthotopic tumors with representative images of tumors harvested from one mouse cecum. C: Representative H&E snapshots of RSC and CBC orthotopic tumors after 5 weeks *in vivo*, magnified individual tumors (top) and whole-cecum "swiss rolls" (below), scale = 200µm and 1000µm, green line marks the muscularis mucosae. D: H&E staining and image of mesenteric lymph node filled with tumor cells found in the CBC orthotopically injected mouse from (C), scale bar = 500µm. E: H&E staining of a mesenteric lymph node filled with tumor cells, found in another CBC-injected mouse, scale = 200µm. F: Image of liver dissected from a CBC orthotopically injected mouse (in the scRNA-seq cohort) with likely indication of metastatic tumor growth.

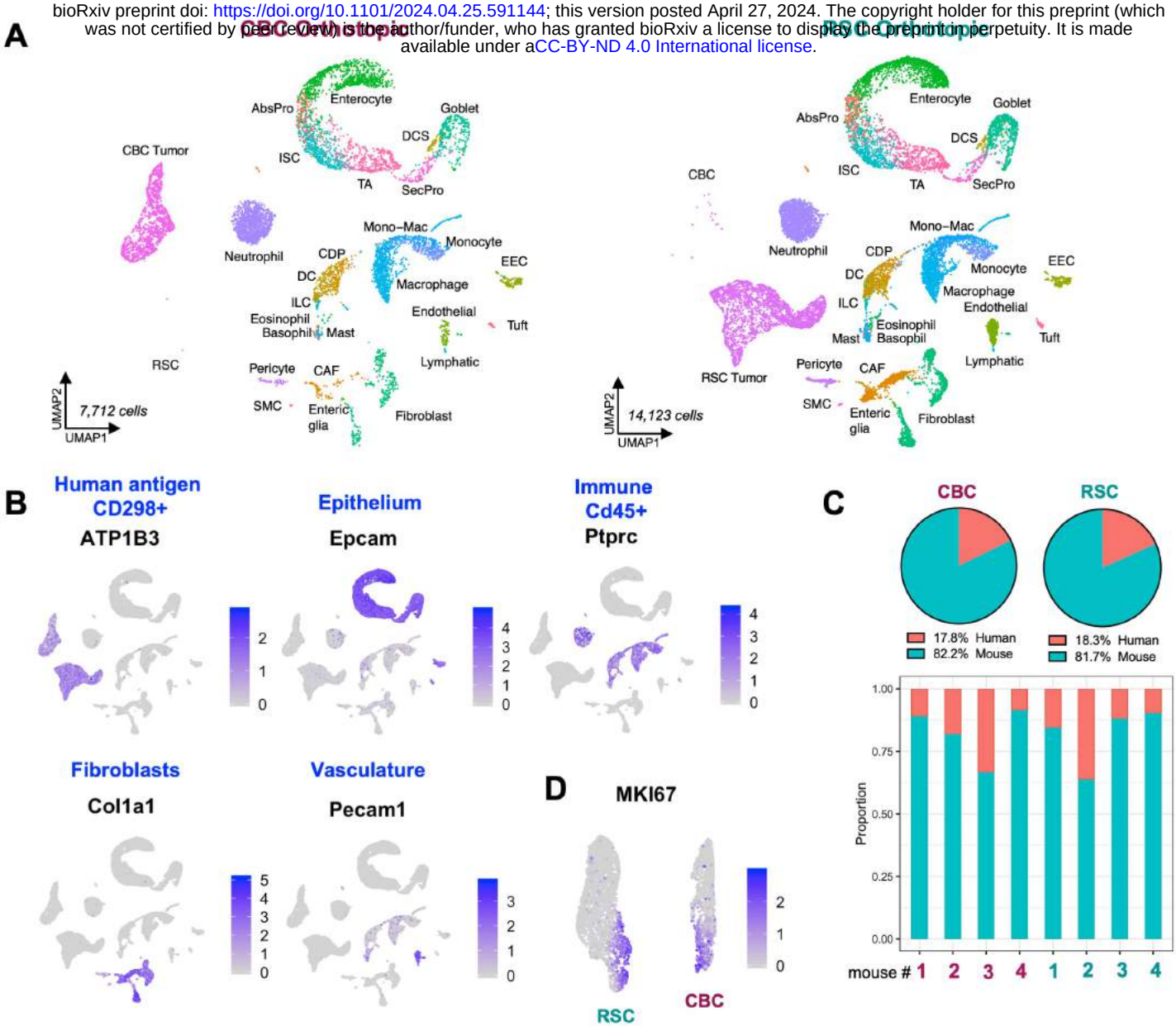

Figure S14, related to Figure 4: Single cell sequencing of orthotopic xenografts reveals a diverse and expanded tumor microenvironment that dominates the tumor setting.
A: UMAP clustering of all mouse and human cells captured in CBC and RSC orthotopic tumors, n = 4 each subtype. B: Gene expression plots of marker genes for the major cellular compartments in orthotopic tumors. SW480 human tumor cells are identified by human specific antigen CD298 (*ATP1B3).* C: Proportion of human tumor to mouse TME on average (pie chart) and in each replicate (below). D: Gene expression plot of a cell cycling biomarker, *MKI67,* in the human tumor compartment.

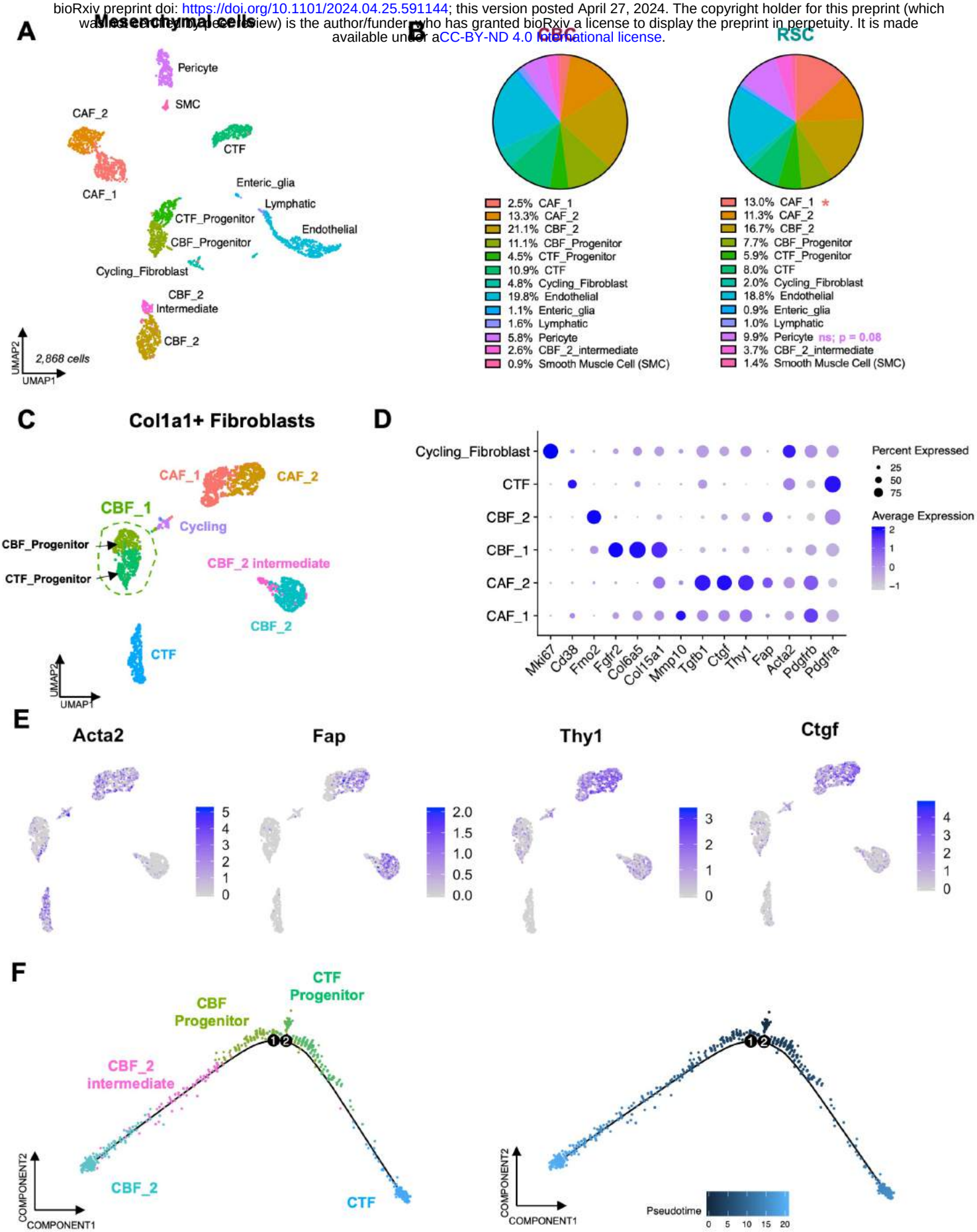

Figure S15, related to Figure 5: Identification of normal and cancer-associated fibroblast populations.

Figure S15, related to Figure 5: Identification of normal and cancer-associated fibroblast populations.
A: UMAP clustering of all mesenchymal cells in orthotopic tumors. B: Pie charts showing proportional compositions of mesenchymal cell types in CBC and RSC orthotopic tumors; P value = * < 0.05 (Student's t test). C: UMAP clustering of *Col1a1*+ mesenchymal cells subsets all normal and cancer-associated fibroblast (CAF) populations. D: DotPlot of intestinal fibroblast markers: differential *Pdgfra* expression distinguishes crypt top fibroblast (CTF) from crypt bottom fibroblast (CBF) populations (Brügger et al., 2020; ref. 29). The universal fibroblast progenitor marker *Col15a1* (Buechler et al., 2021; *Nature* 593(7860):575-579) identifies the CBF_1 cluster as a bi-potent progenitor to CTF and CBF_2 clusters. E: Gene expression plots of CAF and myofibroblast marker genes (*Acta2*/SMA, *Fap*, *Thy1, Ctgf)*. Since *Fap* is co-expressed by CAFs and normal CBF_2 fibroblasts, *Thy1* and *Ctgf* are better, exclusive gene markers of CAFs. F: Monocle2 analysis orders normal crypt fibroblast populations by "pseudotime" with the two CBF_1 sub-clusters distinctly divided: the darker green cluster appears to be closely connected to the CTF population and is placed at the beginning of 'pseudotime', therefore we refer to this initiating Monocle population as "CTF_Progenitor"; the lime green cluster is situated on a path that leads to the CBF_2 populations and is therefore referred to as "CBF_Progenitor".

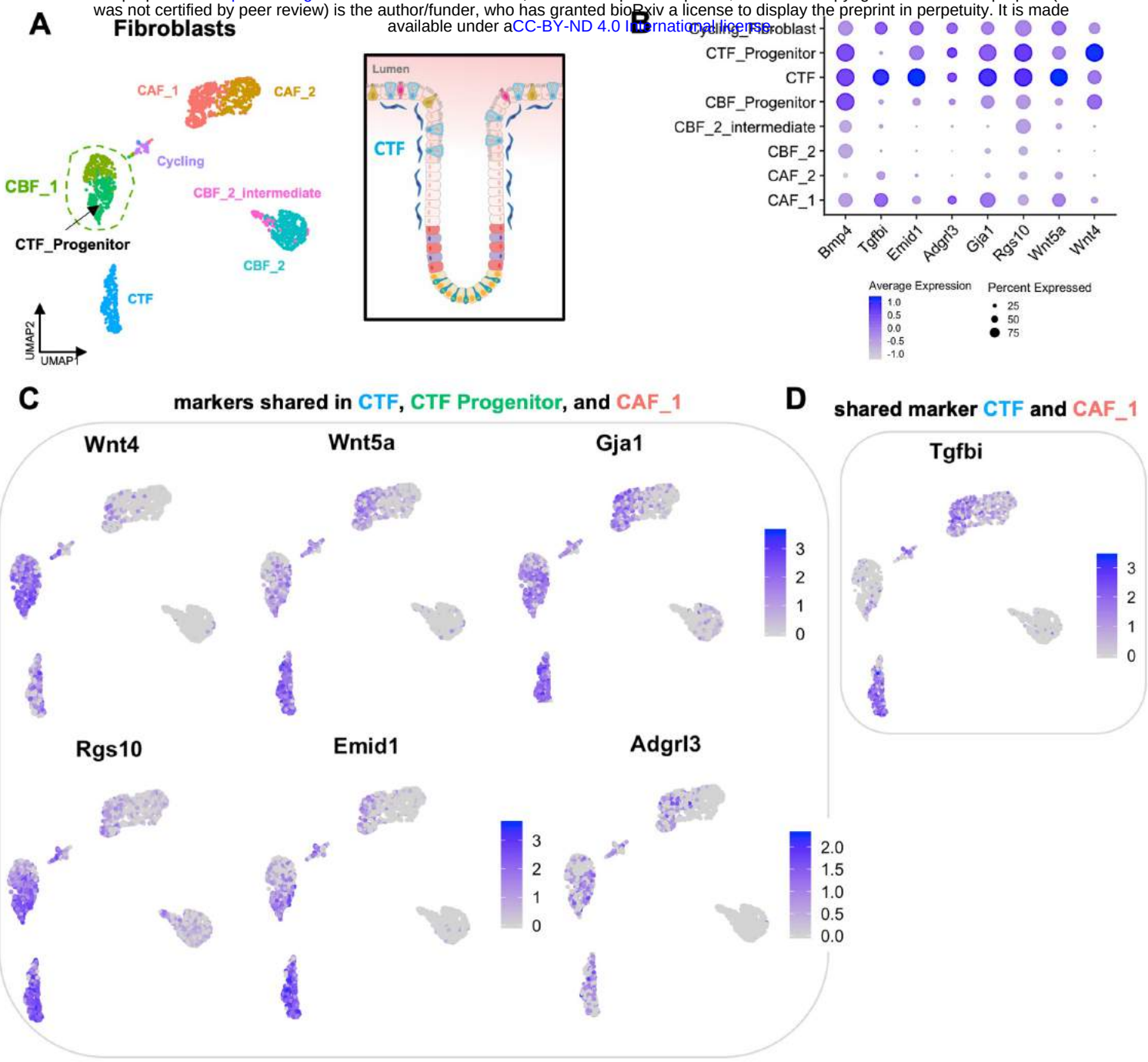

Figure S16, related to Figure 5: Shared gene expression relationships between Crypt Top Fibroblasts and CAF_1 cells.

A: UMAP clustering of fibroblast states, highlighting the two transcriptionally distinct sub-populations within the CBF_1 cluster, indicating here the CTF_Progenitor state. B: DotPlot of genes co-expressed between CTF, CTF_Progenitor and CAF_1 populations. C: Gene expression plots of biomarkers co-expressed in CTF, CTF_Progenitor and CAF_1 populations (*Wnt4, Wnt5a, Gja1, Rgs10, Emid1, Adgrl3*). D: Gene expression plot of shared *Tgfbi* expression in CTF and CAF_1 populations.

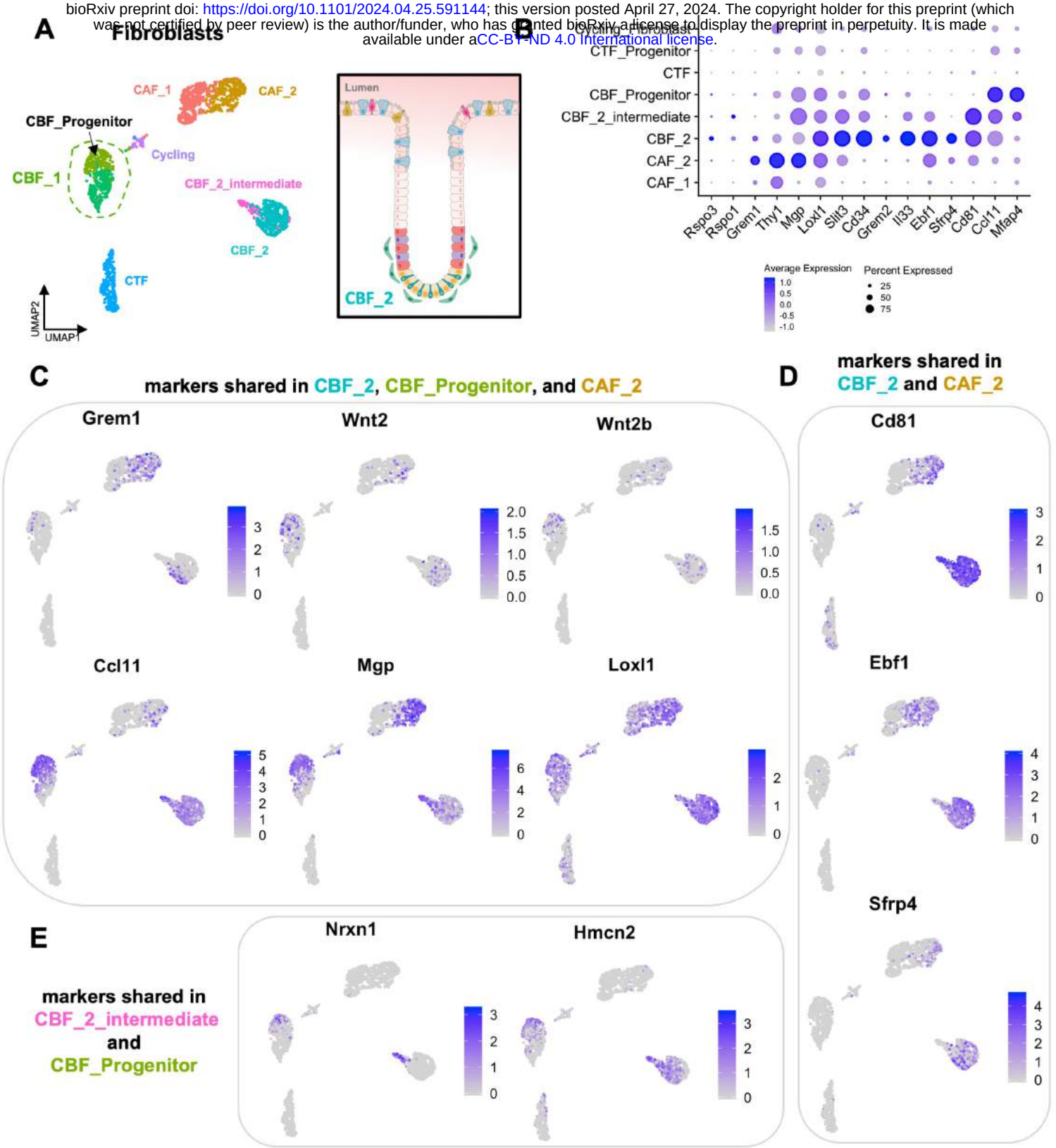

Figure S17, related to Figure 5: Shared gene expression relationships between Crypt Bottom Fibroblasts and CAF_2 cells.

A: UMAP clustering of fibroblast states, highlighting the two transcriptionally distinct sub-populations within the CBF_1 cluster, indicating here the CBF_Progenitor state. B: DotPlot of genes co-expressed in CBF_2 sub-populations and CAF_2 cells. C: Gene expression plots of genes co-expressed in CBF_Progenitor, CBF_2, and CAF_2 populations include genes for secreted factors (*Grem1, Wnt2, Wnt2b, Ccl11, Mgp*). D: Gene expression plots of genes co-expressed in CBF_2 and CAF_2 populations (*Fap, Cd81, Ebf1, Sfrp4*). E: Gene expression plots of genes co-expressed in CBF_2_intermdiate and CBF_Progenitor populations (*Nrxn1, Hmcn2, Gucy1a1, Ces1d*). CBF_2 is considered to be the telocyte population due to expression of biomarkers: *Cd34, Grem1, Grem2, Wnt2, Wnt2b, Rspo1* and *Rspo3*.

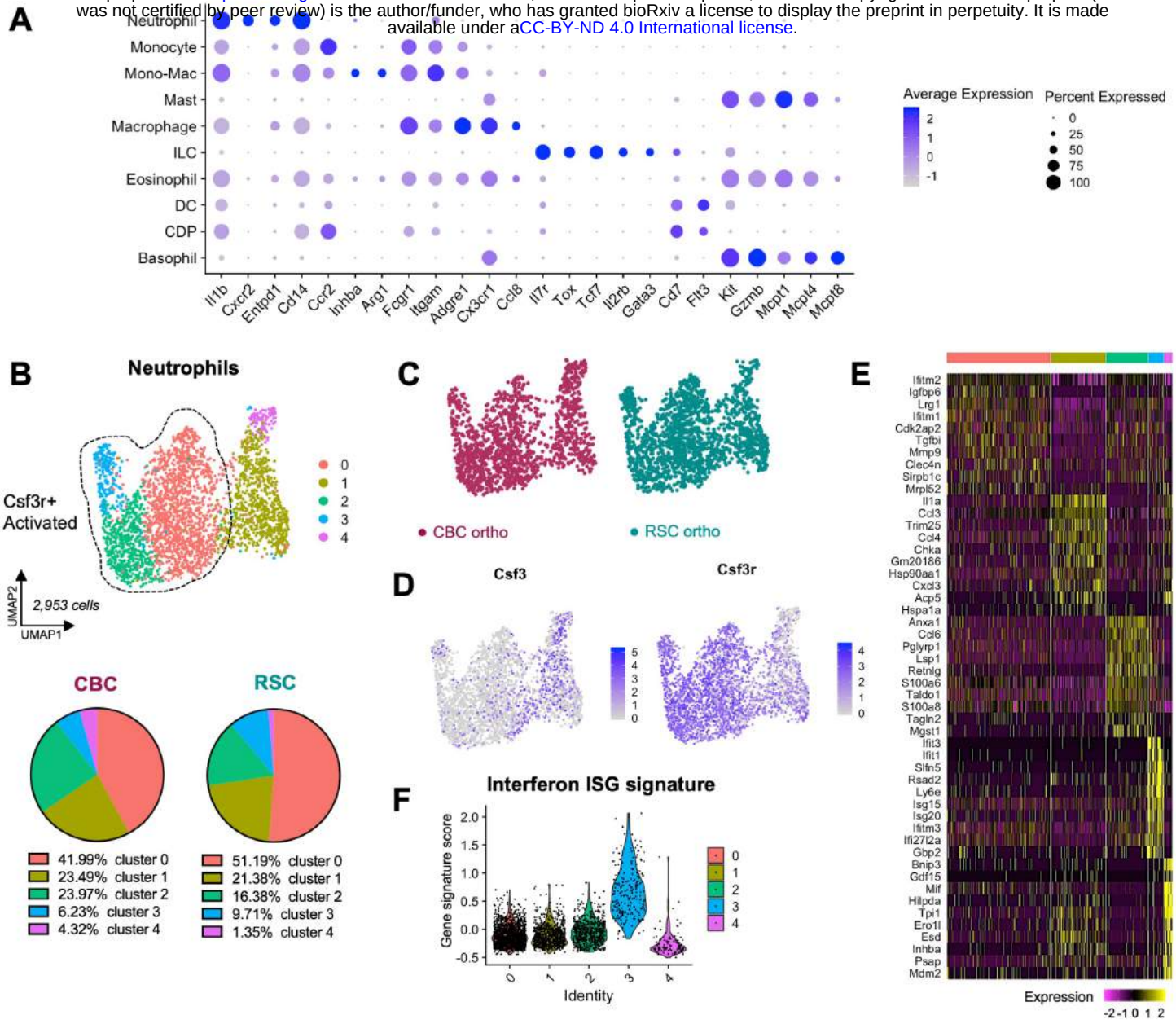

Figure S18, related to Figure 6: **Neutrophils are the most abundant immune cell type in the orthotopic setting but little difference is observed between tumor subtypes.**

A: DotPlot of marker genes for the immune cell types found in the orthotopic tumor microenvironment. B: UMAP clustering of neutrophils, with pie charts showing siimilar proportional compositions of neutrophil subclusters between tumor subtypes. C: UMAP clustering of neutrophils colored by subtype-specific xenograft. D: Gene expression plots of resting (*Csf3*+) and activated (*Csf3r*+) neutrophil states (Park et al., 2022; *Front Oncol.*12:932608). E: Heatmap of marker genes distinguishing neutrophil clusters. F: Violin plot of the Interferon Stimulated Gene (ISG) signature scoring amongst neutrophil clusters, the *Csf3r*+ population (cluster 3) has enriched expression.

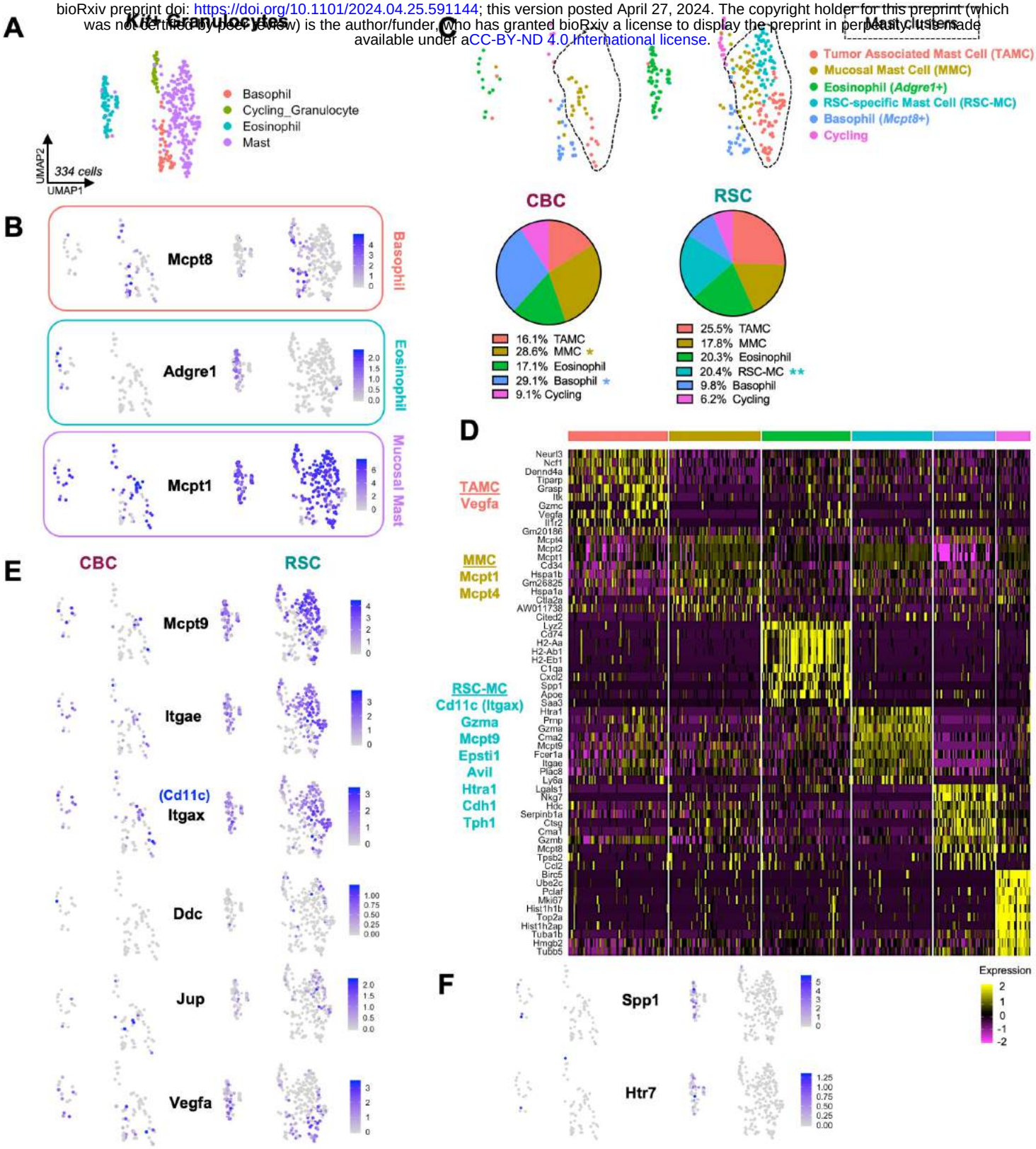

Figure S19, related to Figure 6: Mast cells exhibit multiple phenotypes in the orthotopic tumor microenvironment with a novel population found exclusively in RSC tumors.

A: UMAP clustering of *Kit*+ granulocytes (mast, eosinophil, basophil) present in orthotopic tumors. B: Gene expression plots of marker genes identifying basophil, eosinophil and intestinal mucosal mast cell populations in each subtype-specific xenograft. C: UMAP of *Kit*+ granulocytes colored by transcriptional state, with pie charts highlighting proportional differences of populations in tumor subtypes. Mast cells comprise three distinct transcriptional populations, one of which is found exclusively in RSC tumors (RSC-MC). D: Heatmap of marker genes distinguishing mast cell states with key marker genes of the novel RSC-MC population is listed in teal. E: Gene expression plots of upregulated genes enriched in RSC mast cells. F: Gene expression plots of genes upregulated in RSC eosinophils. P values = * < 0.05, ** < 0.01 (Student's t test).

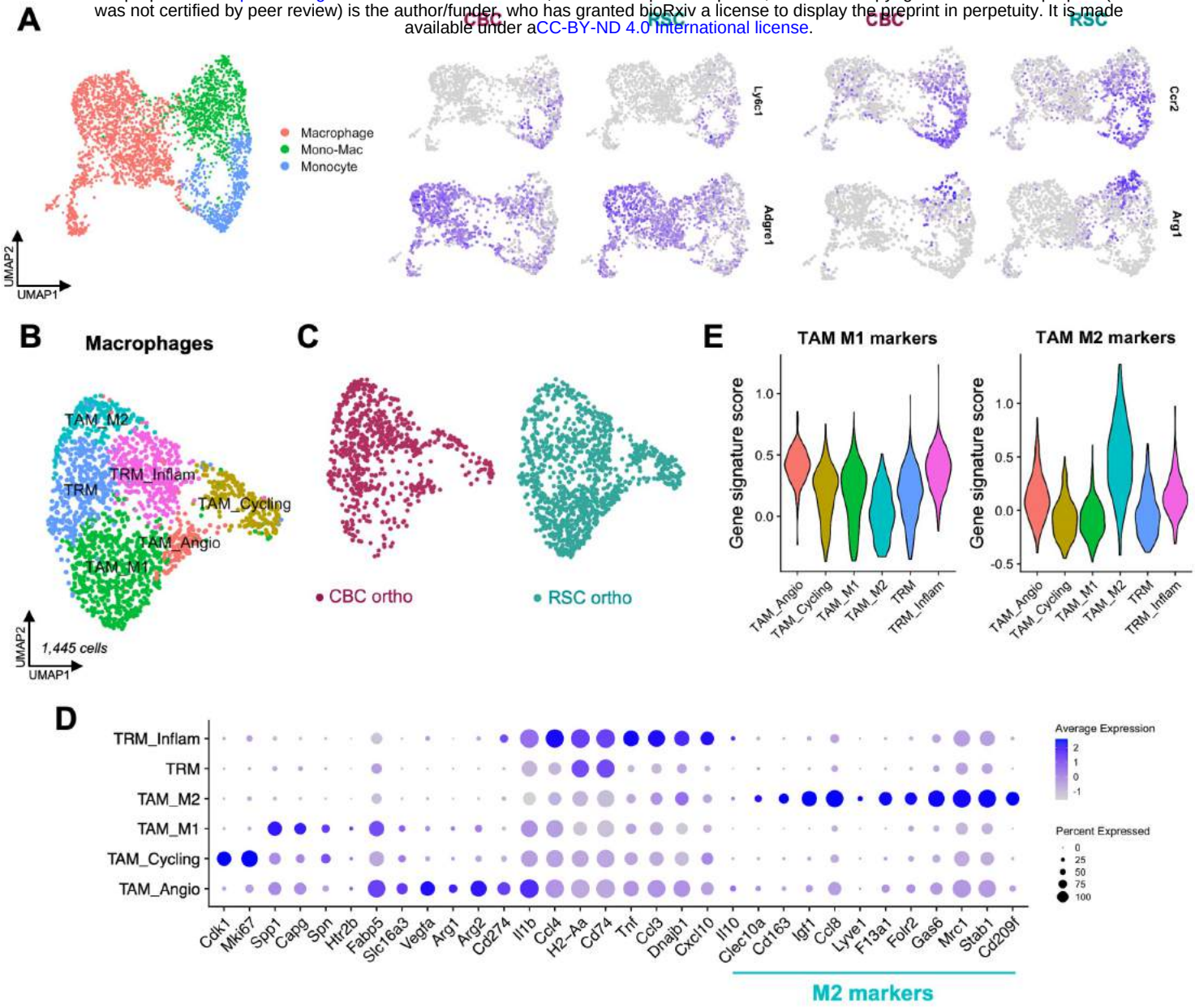

Figure S20, related to Figure 6: Monocytic immune cells are a large, expanded compartment in the orthotopic microenvironment including several tumor associated macrophage states.
A: UMAP clustering and gene expression plots showing *Ly6c1*+ monocytes, *Adgre1*+ macrophages, and an intermediate *Ccr2*+ monocyte-derived macrophage (Mono-Mac) population, with a subset expressing *Arg1*. B: UMAP clustering of tumor associated macrophage (TAM) and tumor resident macrophage (TRM) states. C: UMAP of macrophages states colored by subtype-specific xenograft. D: DotPlot of marker genes distinguishing each TAM and TRM population. Tissue Resident Macrophages (TRMs), identified by a lack of polarized M1/M2 markers and heightened expression of MHC-II markers *H2-Aa* and *Cd74*, were a distinct population found in both tumor subtypes with a subset expressing multiple inflammatory cytokines (TRM_Inflam; *Il1b, Ccl3, Ccl4, Tnf, Cxcl10, Dnajb1*).
E: Violin plot of gene signature scoring of M1 and M2 associated TAM marker genes (see Supplemental Data 3 for gene lists).

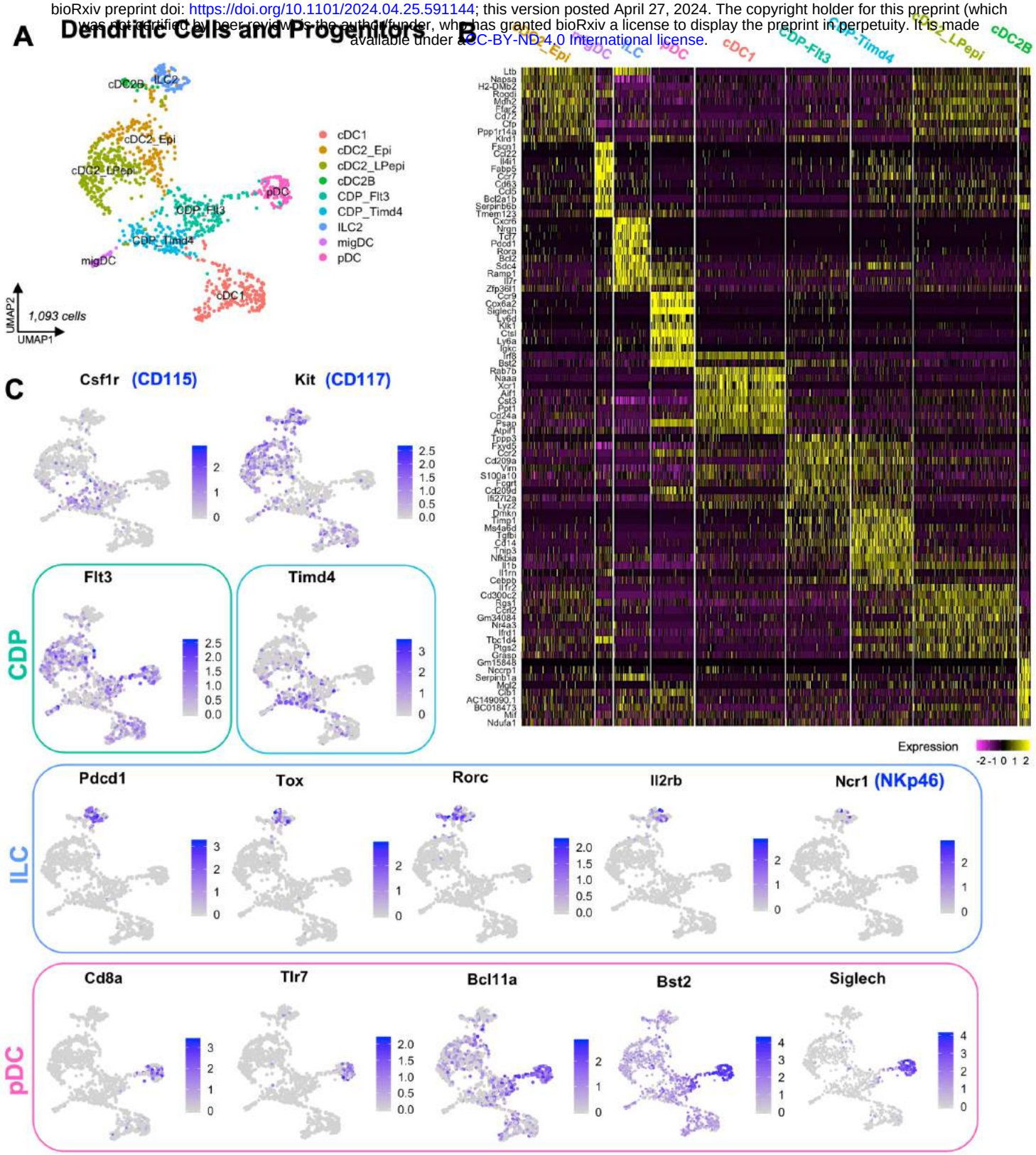

Figure 21, related to Figure 6: **The orthotopic tumor microenvironment contains many types of dendritic cells with distinct transcriptional profiles.**

A: UMAP clustering of dendritic cell (DC) subtypes: conventional DC 1 and 2 (cDC1, cDC2) with additional cDC2 heterogeneity, migratory DC (migDC), plasmacytoid DC (pDC), common DC progenitor (CDP), and innate lymphoid group 2 cells (ILC2). B: Heatmap of marker genes identifying each dendritic cell and progenitor subpopulation. C: Gene expression plots of biomarkers of dendritic cell (DC) subpopulations: CDP cells marked by CD115+;CD117^{lo} express different levels of *Flt3* and *Timd4*. Innate lymphoid cells (ILCs) are an early precursor to the adaptive immune compartment and express genes involved with T-cell (*Pdcd1, Tox, Rorc*) and NK cell (*Il2rb, Ncr1*/NKp46) functions. Plasmacytoid DCs (pDC) have unique markers (*Cd8a, Siglech* and *Tlr7)* and more strongly express *Bst2* and *Bcl11a* compared with other DC subpopulations.

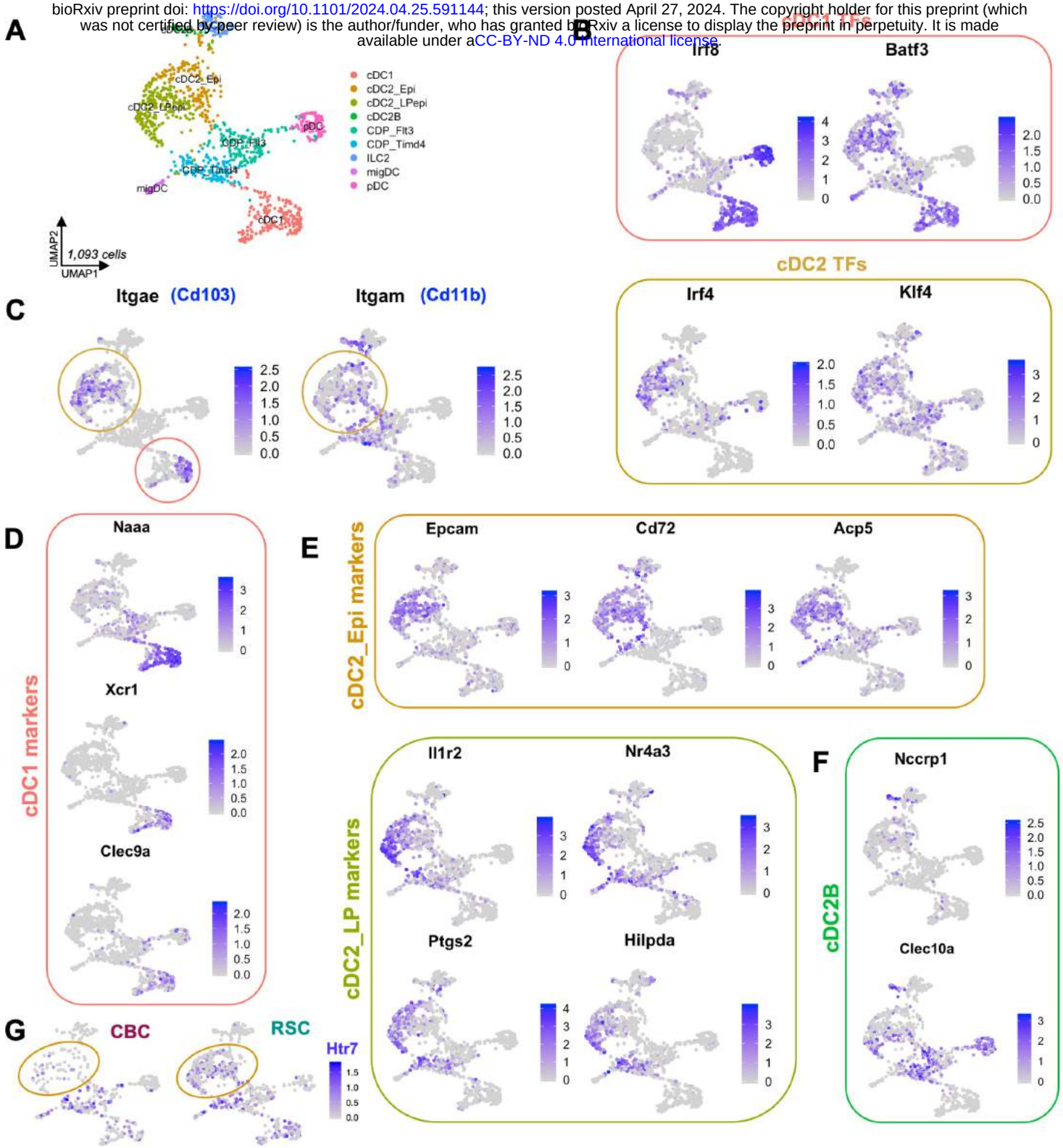

Figure S22, related to Figure 6: Conventional dendritic cells exhibit the most diversity amongst dendritic cell subtypes in the orthotopic tumor microenvironment.

A: UMAP clustering of dendritic cell (DC) subtypes: conventional DC 1 and 2 (cDC1, cDC2, cDC2B) with additional cDC2 heterogeneity defined in (E), migratory DC (migDC), plasmacytoid DC (pDC), common DC progenitor (CDP), and innate lymphoid group 2 cells (ILC2). B: Gene expression plots of master transcription factor regulators for cDC1 (*Irf8*, *Batf3*) and cDC2 (*Irf4*, *Klf4*) lineages. C: Gene expression plots of intestinal specific cDC marker genes for cDC1 (Cd103+ Cd11b-) and cDC2 (Cd103+ Cd11b+) populations. D: Gene expression plots of cDC1 marker genes with distinctive expression of migratory marker (*Xcr1*). E: Gene expression plots of genes expressed in cDC2 subtypes associated with Epithelial (cDC2_Epi) or Lamina Propria (cDC2_LP) compartmental localization (markers from Rivera et al. 2022, ref. 32). F: Gene expression plots of genes identifying cDC2B cells (*Clec10a and Rorc*). G: Gene expression plot of Htr7 expression in cDC2 cells, enriched in RSC tumors.

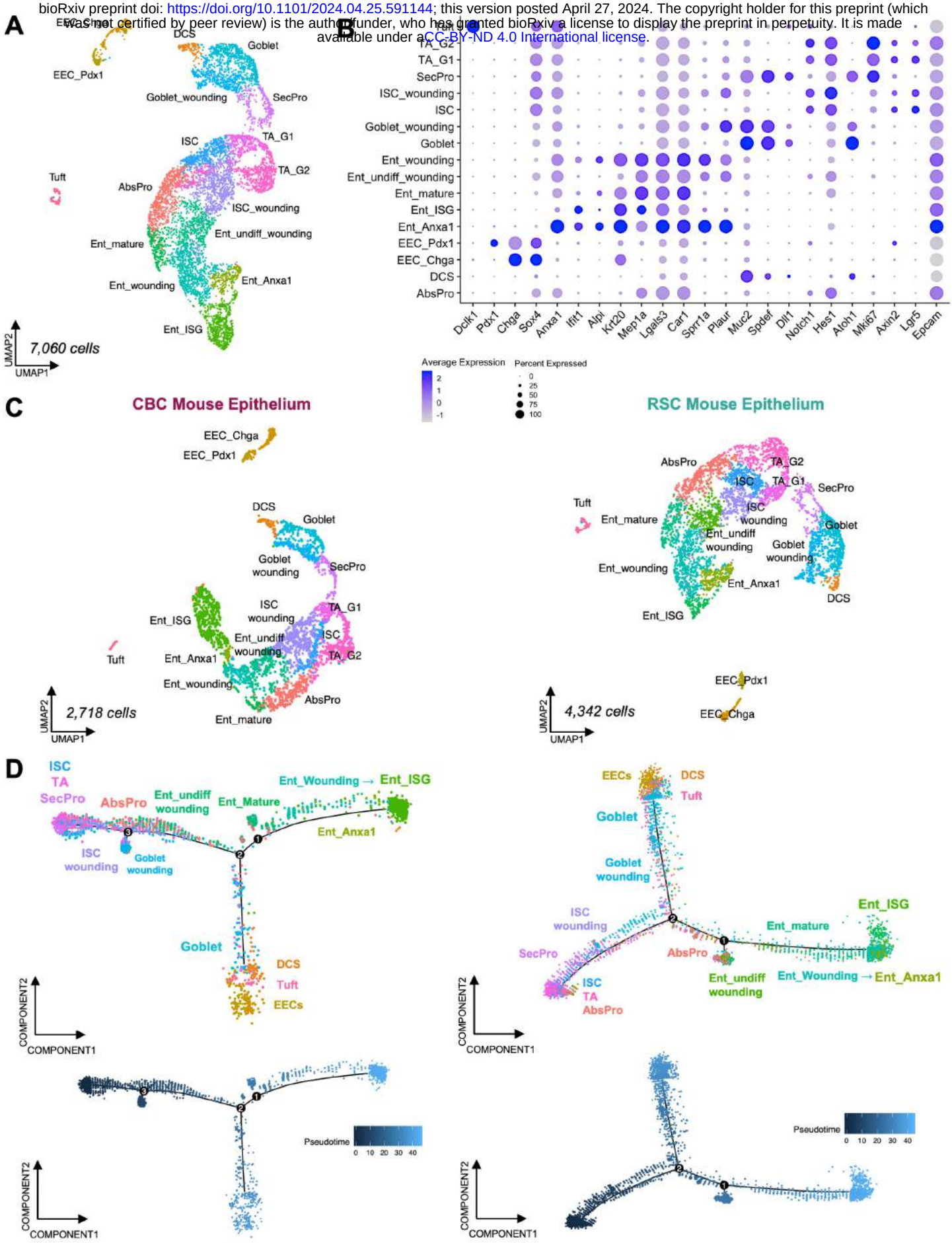

Figure S23, related to Figure 7: Monocle pseudotime analysis reveals unique tumor subtype-specific patterns of epithelial wounding and differentiation.

Figure S23, related to Figure 7: Monocle pseudotime analysis reveals unique tumor subtype-specific patterns of epithelial wounding and differentiation.

A: UMAP clustering of *Epcam*+ mouse epithelial cells and wounded counterparts in orthotopic tumors: intestinal stem cells (ISCs), Absorptive Progenitors (AbsPro), Secretory Progenitors (SecPro), immature *Krt20*- enterocytes (Ent_undiff_wounding), mature *Krt20*+ non-wounded (Ent_mature) and wounded (Ent_wounding) enterocytes, and wounded-specific populations of *Anxa1*+ (Ent_Anxa1) and interferon stimulated gene expressing (Ent_ISG) enterocytes, normal and wounded goblet cells, tuft cells, and *Chga*+ enteroendocrine (EEC_Chga) and *Pdx1*+ enteroendocrine (EEC_Pdx1) cells. B: DotPlot showing biomarkers of intestinal epithelial cell populations and genes involved in lineage specification and differentiation. C: UMAP clustering of mouse epithelial cells separated by CBC (left) and RSC (right) orthotopic tumor identity. D: Monocle2 analysis of CBC (left) and RSC (right) tumor associated mouse epithelial populations orders cells by transcriptional similarities creating a lineage differentiation trajectory, measured by 'pseudotime' (bottom graphs). The ISC compartment and early progenitors mark the beginning of 'pseudotime' and wounded differentiated populations in CBC tumors generally lie closer in pseudotime to the ISC populations, whereas wounded differentiating populations (enterocytes and goblet cells) in RSC tumors are farther along the pseudotime trajectory indicating less damage and an earlier stage of tumor-induced wounding.

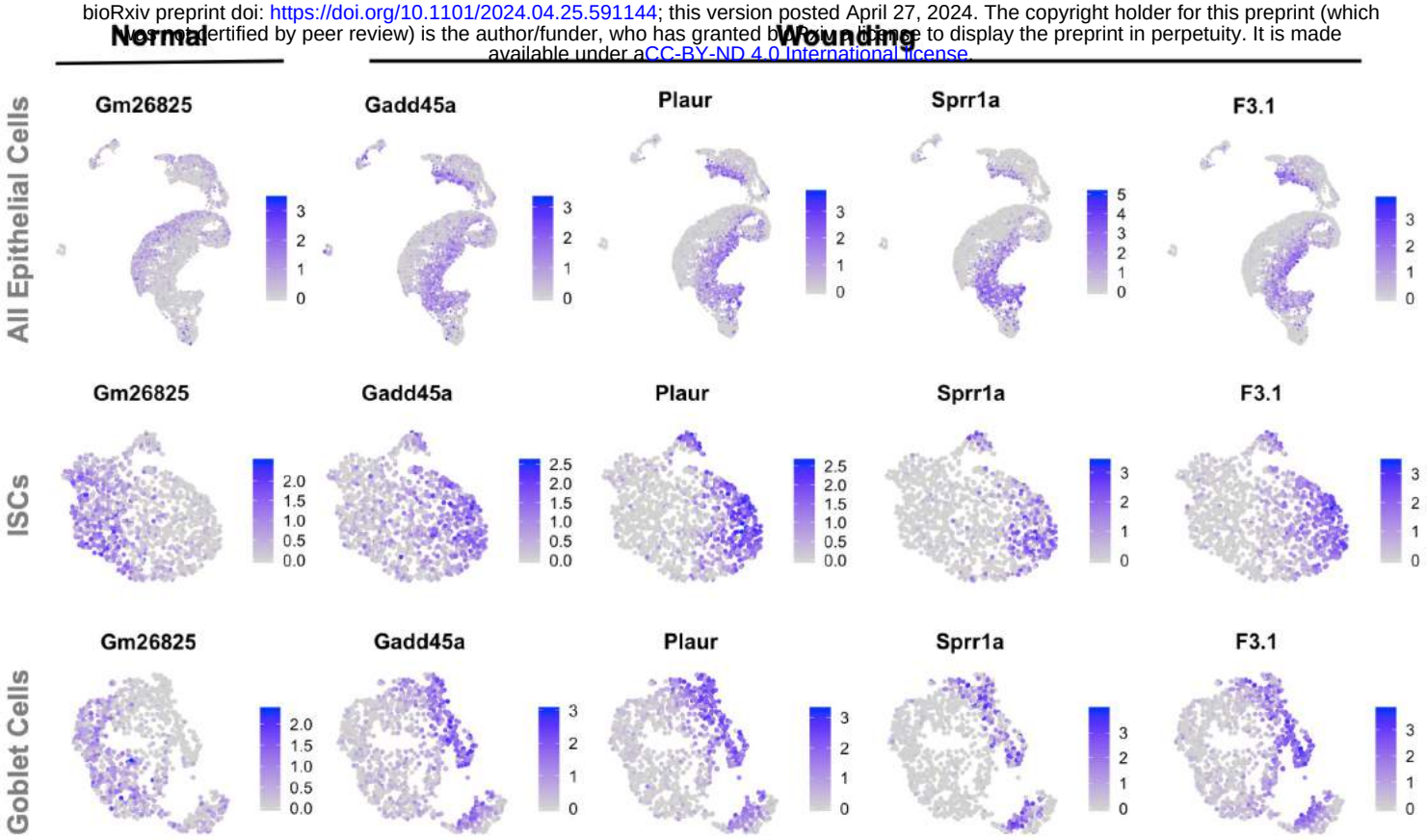

Figure S24, related to Figure 7: Biomarkers of normal and wounding-associated genes expressed in multiple mouse epithelial cell populations.
UMAPs of all mouse epithelial cells (top), the ISC compartment (middle), and the goblet population (bottom) have distinct expression of normal and wounding-associated genes. *Gm26825*, a lncRNA, is expressed in non-wounded (normal tissue) populations of epithelial cells from both tumor subtypes, while *Gadd45a*, *Plaur Sprr1a* and *F3.1* are examples of genes upregulated in tumor-induced wounding states of mouse epithelia. The large wounded enterocyte population is evident in the lower right of the UMAP of all epithelial cells.

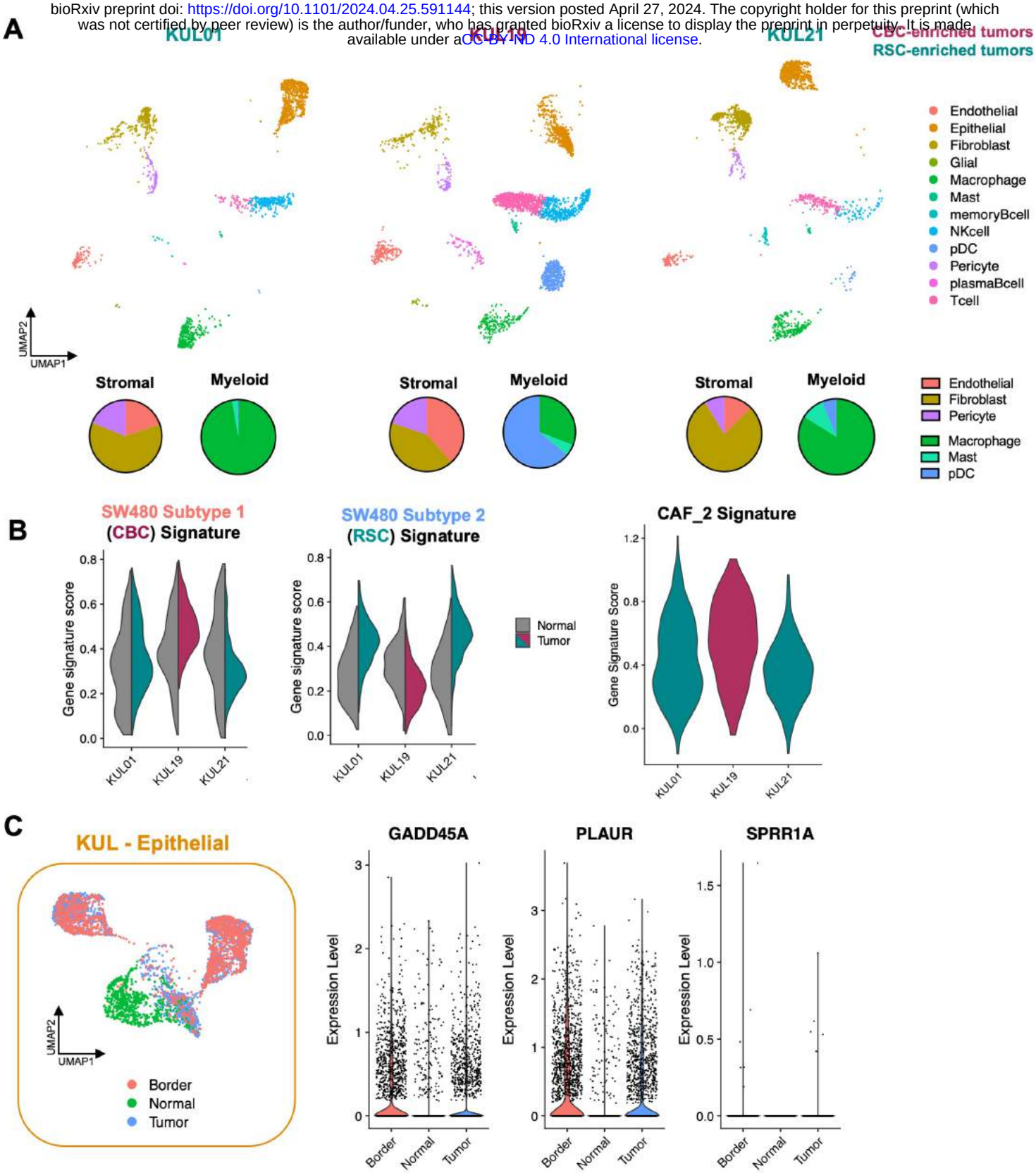

Figure S25, related to Figure 2: CRC patient TME correlates with SW480 subtype-specific TME compositions and phenotypes.

A: UMAP clustering of the tumor microenvironment from Belgian (KUL) patient tumor biopsies. Pie charts indicate differing compositions of stromal and myeloid cells in CBC- and RSC-enriched patient tumors. B: Violin plots of gene scoring for SW480-derived CBC and RSC signatures show that CBC-enriched patient tumors have CAFs with a higher CAF_2 signature, which correlates with a worse prognosis. C: Epithelial cells from normal, border, and tumor biopsies of Belgian (KUL) patients show that bystander border but not distant normal tissue expresses wound-specific biomarkers *GADD45A*, *PLAUR*, and *SPRR1A*.

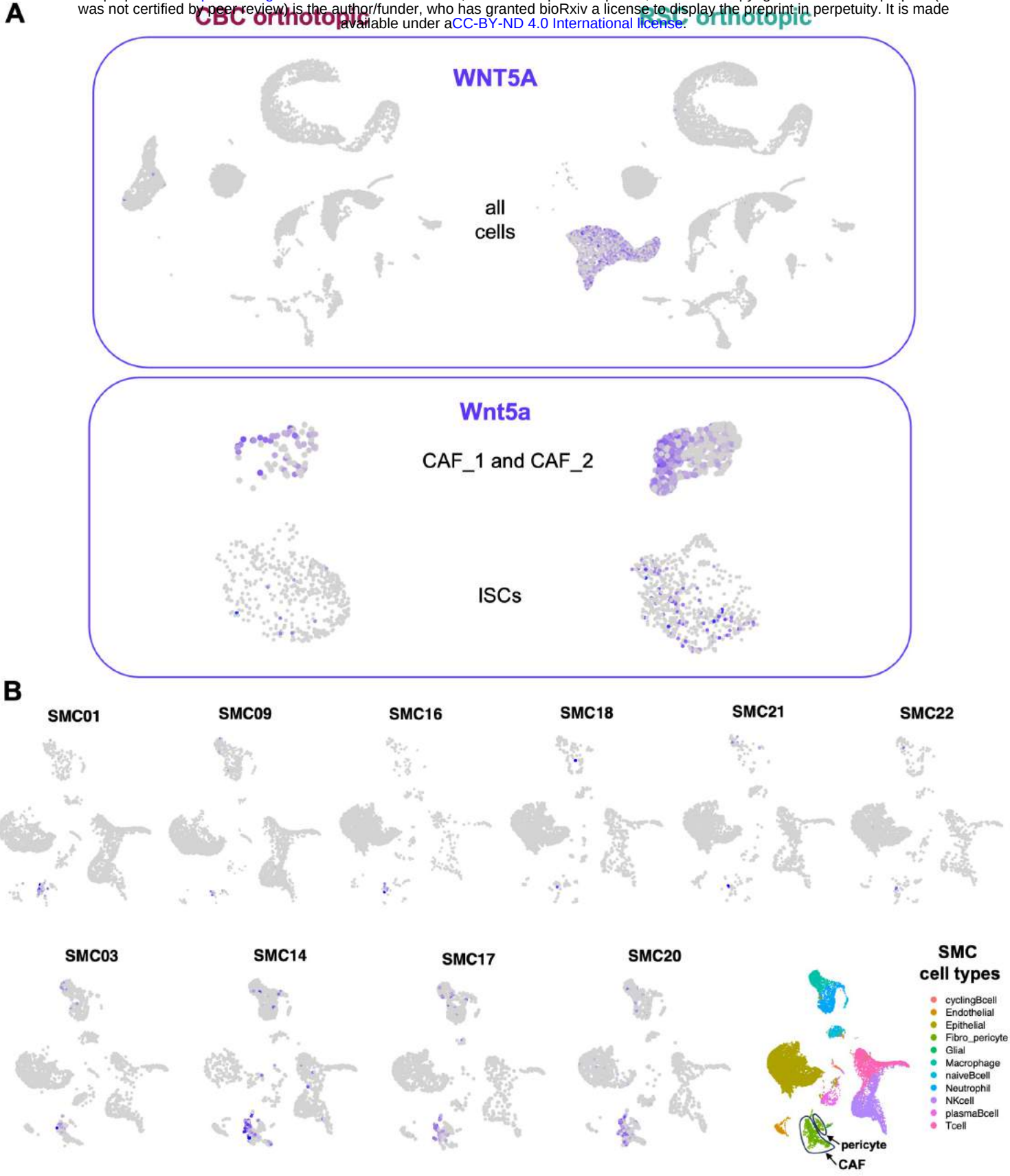

Figure S26: Inflammatory ligand WNT5A/Wnt5a is predominantly expressed in RSC tumors.
Gene expression plots of non-canonical WNT expression in the tumor microenvironment show the major sources of this inflammatory signal come from tumor cells (specifically WNT5A from the RSC subtype), cancer associated fibroblasts (CAFs; specifically CAF_1 in the RSC TME), and Intestinal Stem Cells (ISCs; predominantly in the RSC TME) in the orthotopic tumor model (A), and WNT5A is expressed by CAFs in RSC enriched patient (SMC14, SMC17, SMC20) tumors (B).